Biophysical Journal
Article

Biophysical Society

A Database of Predicted Binding Sites for Cholesterol on Membrane Proteins, Deep in the Membrane

Anthony G. Lee[1,*]
[1]Centre for Biological Sciences, University of Southampton, Southampton, United Kingdom

ABSTRACT The outer membranes of animal cells contain high concentrations of cholesterol, of which a small proportion is located deep within the hydrophobic core of the membrane. An automated docking procedure is described that allows the characterization of binding sites for these deep cholesterol molecules on the membrane-spanning surfaces of membrane proteins and in protein cavities or pores, driven by hydrogen bond formation. A database of this class of predicted binding site is described, covering 397 high-resolution structures. The database includes sites on the transmembrane surfaces of many G-protein coupled receptors; within the fenestrations of two-pore K^+ channels and ATP-gated P2X3 channels; in the central cavities of a number of transporters, including Glut1, Glut5, and P-glycoprotein; and in deep clefts in mitochondrial complexes III and IV.

INTRODUCTION

Membrane proteins play a central role in the physiology of the cell, particularly as receptors, channels, and transporters. High-resolution structural information is now available for many of these proteins in isolation, but much less is known about how they interact with the lipid bilayer component of the membrane. The membrane-spanning surfaces of membrane proteins are often pictured as bland and featureless, but in fact, the surfaces are rough, containing many crevasses and holes, and are dotted with atoms capable of forming hydrogen bonds with small polar molecules located within the hydrophobic core of the membrane (1). Some of these surface-exposed atoms will be involved already in hydrogen bonding with other atoms within the protein, and any additional, intermolecular hydrogen bonds that might form will be relatively weak (2), but others will have no intramolecular partners and could therefore form strong hydrogen bonds with a suitable partner. Fig. 1 *A* shows the hydrophobic region of the agonist-free β_2 adrenergic receptor (3); this region contains, exposed on the surface and not involved in intramolecular hydrogen bonding, four O and nine N atoms from the backbone, three side-chain NH groups and seven side-chain OH groups, and three methionine S atoms and five side-chain SH groups.

One hydrophobic molecule capable of hydrogen bonding to the transmembrane (TM) surface of a membrane protein is cholesterol, which typically makes up between 25 and 50 mol% of the lipid molecules in the plasma membranes of animal cells (4–6). Most of these cholesterol molecules are located with their −OH groups close to the glycerol backbone region of the lipid bilayer, with their hydrophobic rings in the hydrophobic core of the bilayer. Correspondingly, all membrane-protein crystal structures that include resolved cholesterol molecules show the bound cholesterol molecules with their −OH groups in what, in a lipid bilayer, would be the glycerol backbone region, as shown in Fig. S1 for the human purinergic receptor $P2Y_{12}$ (7). In some cases, the −OH group of the resolved cholesterol molecule is hydrogen bonded to the protein, as in the β_2 adrenergic receptor, in which the hydrogen bond is to an Arg residue, part of a suggested cholesterol consensus motif CCM; two other possible cholesterol-binding motifs, CRAC and CARC, also involve an Arg (or Lys) residue (3,8). In other cases, the resolved cholesterol molecules do not form any hydrogen bonds with the protein, as for the $P2Y_{12}$ receptor shown in Fig. S1, and it is likely that hydrogen bonds are formed to lipid or water molecules in the lipid glycerol backbone and headgroup regions.

However, not all the cholesterol molecules in a biological membrane are located with their −OH groups at the membrane-water interface; neutron diffraction studies and molecular dynamics simulations have shown a small

Submitted April 9, 2018, and accepted for publication June 19, 2018.
*Correspondence: agl@soton.ac.uk
Editor: D. Peter Tieleman.
https://doi.org/10.1016/j.bpj.2018.06.022

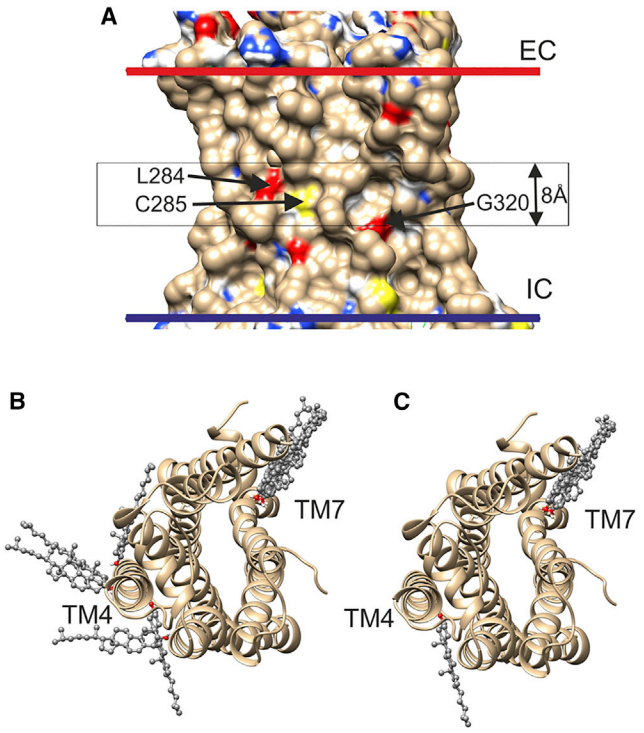

FIGURE 1 Docking of cholesterol to the agonist-free β_2 adrenergic receptor (PDB: 3D4S). (*A*) The membrane-spanning surface shows the locations of surface-exposed oxygen (*red*), nitrogen (*blue*), and sulfur (*yellow*) atoms not involved in intramolecular hydrogen bonding. The extracellular (EC) and intracellular (IC) sides of the hydrophobic domain of the membrane surrounding the protein, as given by the OPM database, are shown by red and blue bars, respectively. The central black box shows the position of the 8 Å slab used for docking. The three residues containing surface-exposed, non-hydrogen-bonded O and S atoms located within the box and visible in this view are labeled. (*B*) The 10 most energetically favorable of the 20 docking poses before selection for hydrogen bonding are shown. The view is from the EC side. (*C*) The six poses remaining after selection for cholesterol molecules hydrogen bonding to residues not involved in intramolecular hydrogen bonding are shown. These poses involve hydrogen bonding to Ser161 in TM4 and Gly320 in TM7. To see this figure in color, go online.

proportion of the cholesterol molecules to be located with their −OH groups deep within the bilayer (9–13). It has been estimated that in a protein-containing lipid bilayer, the proportion of cholesterol molecules deep in the bilayer is approximately 3% (1). Any binding between these "deep" cholesterol molecules and the protein surface will be driven by hydrogen bonding, as there is no hydrophobic effect in the hydrophobic interior of the membrane. The standard free energy (ΔG^o) for formation of an intermolecular hydrogen bond in liquid hexane is 5.3 kcals mol^{-1} when calculated in molar concentration units (2,14), equal to 6.5 kcals mol^{-1} when calculated in mole fraction concentration units. Using the relationship $\Delta G^o = -RT\ln K_d$, where K_d is the dissociation constant for the hydrogen bonded complex, gives a value for K_d of 1.8×10^{-5} in mole fraction units. This means that at a mole fraction of deep cholesterol molecules of 0.009 (3% of a total cholesterol mole fraction of 30%), formation of a single hydrogen bond between a protein donor or acceptor atom and a deep cholesterol molecule would result in a >99% probability of the donor or acceptor being hydrogen bonded to a cholesterol −OH group. Cholesterol levels are generally lower in cell organelles than in the plasma membrane and could be different in different regions of a membrane if the membrane contains domains of high and low cholesterol density (13); all these factors could affect the probability of a binding site for cholesterol actually being occupied by cholesterol.

Coarse-grained molecular dynamics (CGMD) simulations of the β_2 adrenergic and A_{2A} adenosine receptors in cholesterol-containing bilayers showed that deep cholesterol molecules did indeed interact with the protein surface deep in the membrane, the interactions being between a cholesterol −OH group and some, but not all, of the potential hydrogen bond partners on the protein surface (1). No cholesterol molecules were observed to interact with the surface only via their hydrophobic moieties, and the best-localized part of a bound cholesterol molecule was observed to be its −OH group, with the ring and chain moieties adopting a range of different positions. Unfortunately, even CGMD simulations need long simulation times to ensure equilibration of the cholesterol molecules (1), making it a daunting task to extend these simulations to the full range of animal membrane proteins for which high-resolution structures are available. However, the fact that binding of deep cholesterol molecules is driven just by the cholesterol −OH group makes a molecular docking approach attractive. A comparison can be made with studies of water binding to proteins using AutoDock Vina (15) because water docking also involves just an −OH group and hydrogen bonding; in a study of a set of structures for bacterial oligopeptide-binding protein A bound to tripeptides, 97% of the crystallographically identified water molecules were correctly identified by docking, with a false positive rate of less than 1 water molecule per structure (16). It is shown here that docking of cholesterol using AutoDock Vina reproduces the results of the CGMD simulations with a speed that makes possible a complete survey of the available crystal structures.

The docking studies reported here suggest that as well as binding sites on the lipid-exposed surfaces of proteins, binding sites also occur in the fenestrations, central pores, and deep clefts present in many membrane proteins. These binding sites, deep in the membrane, will be occupied predominantly by cholesterol molecules because of the limited range of potential hydrogen bond partners to be found dissolved at high concentrations in the central core of the membrane. A number of examples of deep cholesterol binding are explored in some detail, illustrating how widespread such binding is likely to be and its potential importance for membrane protein function. Details of all the dockings are available in the Supporting Material.

METHODS

Crystal structures of animal membrane proteins with resolutions of 3.5 Å or better were identified from the Membrane Proteins of Known 3D Structure (http://blanco.biomol.uci.edu/mpstruc/) and the Orientations of Proteins in Membranes (OPM; http://opm.phar.umich.edu) databases. Protein structure files were downloaded from the OPM database, as this provides structures oriented in a hydrophobic slab representing a lipid bilayer with protein coordinates centered about the middle of the hydrophobic slab (17), convenient for docking.

Docking was performed using AutoDock Vina (15) running under Chimera (18). The cholesterol ligand was prepared for docking with free rotation about the C-OH bond using AutoDock 4 (19). Ligand and solvent molecules were removed from protein structures, and proteins were prepared for docking using the routines provided in Chimera. The search box was chosen centered at $x = 0$, $y = 0$, and $z = 0$ with a length along the z axis of 8 Å and lengths along the x and y axes sufficient to ensure free movement of the cholesterol ligand around the protein. To ensure that the use of three-dimensional grids to represent molecules in AutoDock Vina did not result in binding sites being missed close to the edge of the 8 Å search box, the docking procedure was repeated with a 12 Å search box, rejecting any dockings in which the cholesterol −OH group had an absolute z value greater than 4 Å or, allowing a little "fuzziness" at the boundary, an adjacent C atom (C2–C4) that had an absolute z value greater than 5 Å. Weighting factors for hydrogen bonds and hydrophobic effects were changed from default values of −0.59 and −0.03, respectively, to −2.0 and −0.001, respectively, as described below.

Results were analyzed using in-house Python code. Up to 20 dockings were returned by AutoDock Vina, and these were searched for dockings in which the cholesterol was hydrogen bonded to protein atoms not involved in intramolecular hydrogen bonding using the Chimera hydrogen-bond detector. For symmetric homo-oligomeric proteins, all binding has been assigned to subunit A to aid comparison between data sets. Protein cavities were identified using the CASTp server (sts.bioe.uic.edu/castp/calculation.html) (20).

A table of cholesterol dockings together with associated structure files in Protein Data Bank (PDB) format for downloading are available on the DeepCholesterol web site (https://deepcholesterol.soton.ac.uk).

RESULTS AND DISCUSSIONS

A rapid procedure for detecting deep cholesterol binding sites

The first step in an automated docking procedure is to define the volume around the protein to be searched. In CGMD simulations of the β_2 adrenergic and A_{2A} adenosine receptors in cholesterol-containing bilayers, it was observed that all the deep cholesterol molecules, either free or bound, were to be found in the central 8-Å-thick hydrophobic core of the bilayer (see Fig. 1 *A*) (1). This distinct distribution results from the anchoring of the majority of the cholesterol molecules in a membrane with their −OH groups in the glycerol backbone region of the bilayer (4). Insertion of a rigid cholesterol ring into a phospholipid bilayer reduces the mobility and increases the order of those parts of any fatty acyl chain adjacent to the ring, consequently reducing the partitioning of small molecules into that portion of the bilayer (21,22). The average hydrophobic thickness of a eukaryotic membrane protein as estimated by the OPM database is 31 Å (17), and the hydrophobic thickness of a membrane protein generally matches the hydrophobic thickness of the surrounding lipid bilayer as defined by the distance between the glycerol backbone regions of the two sides of the bilayer (23). With a length for the cholesterol rings of 11.5 Å, the spacing between the ends of the rings, across the bilayer center, will therefore be 8 Å. This central core is also clearly visible in the crystal structure of the G-protein coupled receptor (GPCR) $P2Y_{12}$, which is unique in showing two resolved cholesterol molecules, one on each side of the putative lipid bilayer around the protein (Fig. S1) (7). The two cholesterol −OH groups are located at the two hydrophobic surfaces as defined by the OPM database, and the separation across the bilayer between the ends of the two cholesterol rings is 8.5 Å. CGMD simulations also show that binding of deep cholesterol molecules to a protein surface requires a distortion of the adjacent lipid bilayer, a distortion that will be favored in the central 8 Å core of the bilayer where the groups adjacent to the protein surface will be the flexible C-terminal ends of the phospholipid fatty acyl chains and the chains of the cholesterol molecules (1). For all these reasons, the search volume was chosen to be the central 8-Å-thick section of the membrane; this also has the advantage of avoiding any cholesterol molecules that might bind at the lipid-water interface (Fig. 1 *A*).

Weighting values used in AutoDock Vina for the hydrophobic effect and for hydrogen bonding were derived to describe docking in an aqueous environment (15). In the center of a lipid bilayer, the hydrophobic effect will be very weak, whereas hydrogen bonding will be approximately fourfold stronger than in water (14). New weighting values were therefore developed to match the results of docking to the results of the CGMD simulations described below. It was found that matching required the absolute value for weighting for the hydrophobic effect to be below −0.0012, and that for hydrogen bonding to be between −1.9 and −2.1, compared to the default Vina values of −0.0351 and −0.587, respectively. The weighting value for the hydrophobic effect was therefore set at −0.001, and that for hydrogen bonding at −2.0. Docking energies calculated in AutoDock Vina are based on direct atom-atom interactions and take no account of whether or not a protein atom is involved in intramolecular hydrogen bonding. A Python script was therefore written to select just those dockings that involved hydrogen bonding of the cholesterol −OH group to a non-hydrogen-bonded protein donor or acceptor atom. Free rotation was allowed around the C-OH bond to allow sampling of all possible orientations of the rigid ring relative to the −OH group.

Comparison of docking and CGMD results

The validity of the weighting values used in the docking studies is shown by comparison of the docking results with those obtained previously by CGMD simulation

(Tables 1 and S1). Fig. 1 *B* illustrates the 10 most energetically favorable docking poses from the 20 returned by AutoDock Vina for the agonist-free β_2 adrenergic receptor with no selection based on hydrogen bonding, and Fig. 1 *C* shows the results after selecting from the 20 just those dockings that involved hydrogen bonding to protein atoms not involved in intramolecular hydrogen bonding. The selected docking poses correspond to hydrogen bonding of the cholesterol −OH proton to the backbone carbonyl oxygen of Gly320 in TM helix TM7 and to the side-chain oxygen of Ser161 in TM4 (Table 1).

In CGMD simulations, the protein is represented by a series of beads, each bead typically corresponding to four non-hydrogen atoms (24), allowing the identification of residues close to a cholesterol −OH bead but not allowing the identification of individual atoms involved in hydrogen bonding. In the simulations for the agonist-free β_2 adrenergic receptor, residues with probabilities >25% of being within 5 Å of the −OH bead of a deep cholesterol molecule fell into distinct clusters (Table 1). The first cluster consisted of Gly320 and Phe321; Gly320 contains a non-hydrogen-bonded backbone carbonyl oxygen, whereas Phe321 contains no non-hydrogen-bonded donors or acceptors, consistent with the docking results, which identified Gly320 as the hydrogen bond partner for a deep cholesterol. The second cluster consisted of three residues, of which Ser161 was the only residue with a non-hydrogen-bonded donor or acceptor, again agreeing with the docking results identifying Ser161 as a hydrogen-bond partner for a deep cholesterol (Table 1). Thus, of the eight potential surface-exposed, non-hydrogen-bonded donor and acceptor atoms located in the central 8 Å region of the membrane (Fig. 1 *A*), only two are identified as parts of binding sites for cholesterol by the docking protocol adopted here, and the residues containing these same two atoms are also identified as binding partners in the CGMD simulations. A common feature of many of those atoms that form sites for cholesterol binding is that they are located at the bottoms of concave surface regions or "pockets" as detected by CASTp (Figs. 2 and S2), frequently associated with binding sites (20). Calculations of ligand binding energies in AutoDock Vina are based on a statistical scoring function and so will be less reliable than those calculated using force-field methods. Nevertheless, it is comforting that the calculated binding energies in molar concentration units of 6–7 kcal mol^{-1} (Table 1) are comparable to the experimental value of 5.3 kcals mol^{-1} determined for a single hydrogen bond in a hydrophobic environment (2,14).

TABLE 1 Hydrogen-Bond Partners for Cholesterol in the β_2-Adrenergic Receptor: Comparison of Docking and CGMD results

	Docking		CGMD[a]		
Protein	Residue	E (kcals mol^{-1})[b]	Cluster[c]	Residue[d]	Contact Probability (%)
Agonist-free [3D4S]	G320 [O]	−7.1	1	G320	34
			1	F321	58
	S161 [OG]	−6.1	2	S161	28
			2	V160	38
			2	V206	44
Agonist-Bound [3SN6]	E122 [OE2]/ V206 [O]	−5.8	1	E122	36
			1	I153	27
			1	V157	33

[a]Data from (1).
[b]In molar concentration units.
[c]Cluster numbers from (1).
[d]Residues with a greater than 25% probability of being within 5 Å of a cholesterol −OH group.

CGMD simulations for the agonist-bound β_2 adrenergic receptor show no binding to the two clusters identified for the agonist-free structure and, instead, show most favorable binding to a cluster of three residues including Glu122 (Table 1) (1). This again is consistent with the docking results, which detect hydrogen bonding to the side chain of Glu122, either alone or together with the backbone carbonyl of the adjacent Val206 (Table 1). The CGMD simulations also suggested the presence of a much weaker interaction with a second cluster consisting of Phe208 and Tyr209, both residues individually having a low probability (<25%) of being in contact with a cholesterol −OH bead (1). Neither of these residues contain surface-exposed, non-hydrogen-bonded donor or acceptor atoms and so are not detected as part of a binding site in the docking studies. It is possible that the interaction suggested by the CGMD simulation is an artifact attributable to the "stickiness" of the force fields used in the CGMD simulations (25).

The patterns of interaction detected by CGMD simulations with the A_{2A} adenosine receptor were different from those for the β_2 adrenergic receptor in that the clusters were larger and individual residues showed lower probabilities of interaction with cholesterol (1). Further, whereas cholesterol −OH groups were well localized in the clusters for the β_2 adrenergic receptor, for the A_{2A} adenosine receptor, they occupied a range of positions, sometimes with more than one molecule occupying a position in a cluster at the same time. Of the seven residues in the agonist-free receptor (PDB: 4EIY) and the six in the agonist-bound receptor (PDB: 3QAK) located in the central 8 Å region and containing surface-exposed donor or acceptor atoms not involved in intramolecular hydrogen bonding, none had a high probability of being in contact with a cholesterol −OH bead, average probabilities of contact being 6 and 7%, respectively (1); evidently, binding to the clusters detected by CGMD simulation for the A_{2A} adenosine receptor is not driven by hydrogen bonding. Consistent with these results, docking studies failed to detect any hydrogen-bond-dependent binding of cholesterol for either the 4EIY or 3QAK structures (Table S1). Poorly localized binding of hydrophobic molecules in large hydrophobic cavities has been reported in a variety of proteins, and the interaction clusters identified in the CGMD simulations were suggested

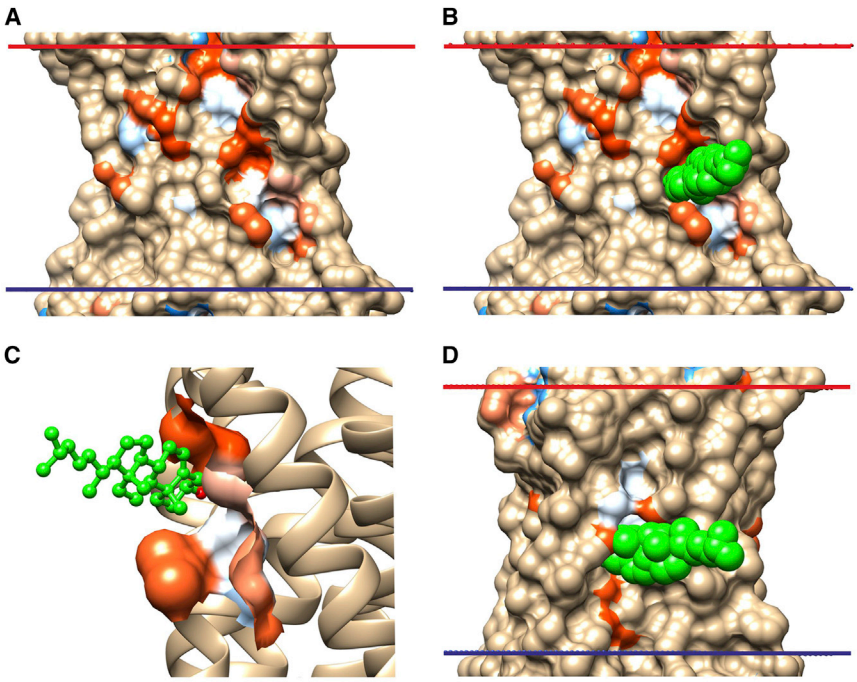

FIGURE 2 The two cholesterol-binding sites identified on the agonist-free β_2 adrenergic receptor. (*A* and *B*) The TM surface with surface pockets identified using CASTp (20) is shown, colored from most hydrophobic (*orange*) to most hydrophilic (*blue*), (*A*) without and (*B*) with a cholesterol molecule (*green spheres*) bound to Gly320. (*C*) An expanded view of the cholesterol binding pocket (cholesterol in *ball* and *stick* representation) is shown. (*D*) The TM surface with a cholesterol molecule bound to Ser161 is shown. To see this figure in color, go online.

to be of this type (1); nonconventional binding sites of this type would not be detected by the docking approach adopted here.

Channels

The two-pore K^+ channels TWIK-1, TRAAK, TREK-1, and TREK-2 have a structure with a narrow selectivity filter on the extracellular (EC) side leading into a large central cavity open to the intracellular (IC) space, as shown in Fig. 3 for TWIK-1 (26–29). The central cavity is connected to the 8 Å core of the lipid bilayer, where the deep cholesterol molecules are found, by openings at the interfaces between the two constituent subunits, just below the selectivity filter (these openings are referred to as fenestrations). The strongest docking observed for TWIK-1 is for a cholesterol molecule with its seven-carbon-long chain in the fenestration, filling its length, with the cholesterol ring and −OH group in the central pore under the selectivity filter and hydrogen bonded to either Thr225 in pore helix 2 or to Leu115 in pore

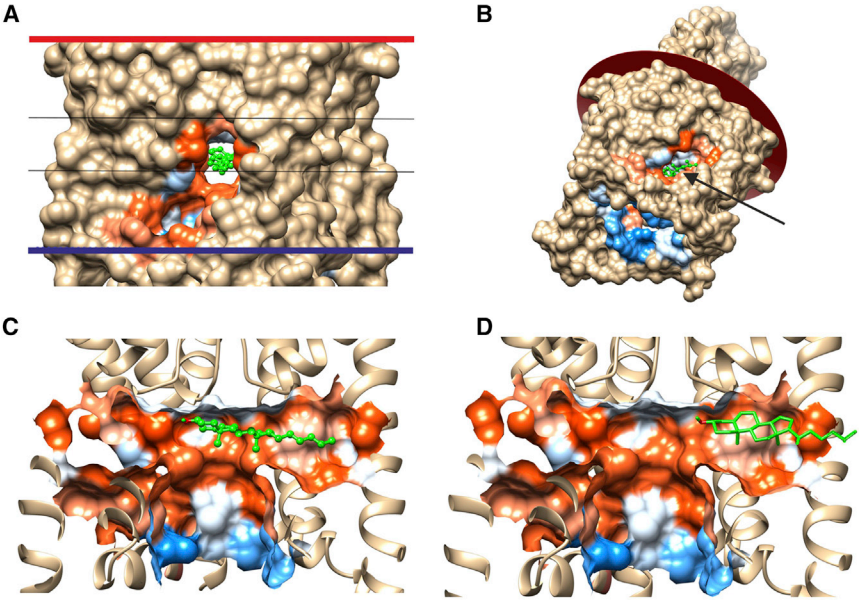

FIGURE 3 Cholesterol binding within fenestrations of TWIK-1 (PDB: 3UKM). (*A*) The TM surface showing the pocket around the central fenestration containing a bound cholesterol (*green*) and the 8 Å search box (*black lines*) is shown. (*B*) A tilted view shows the EC plane and the large cavity exposed on the IC side, with the bound cholesterol (*green*) marked by an arrow. (*C*) A cutaway view shows a bound cholesterol (*green*) in the central pore with its −OH group (*red*) beneath the selectivity filter and its chain in the fenestration. (*D*) A cutaway view shows a cholesterol molecule with its −OH group in the fenestration. To see this figure in color, go online.

helix 1, where it will block ion passage between the selectivity filter and the central cavity (Fig. 3, *A* and *C*; Table S2). The crystal structure of TWIK-1 showed electron density in the fenestration, which could be fitted to an alkyl chain (26). It has been suggested that the chain could belong to a phospholipid molecule, but although a molecular dynamics simulation showed that a phospholipid acyl chain could enter into the fenestration, the chain did not enter far enough to occlude the central pore (30); the binding site for the cholesterol alkyl chain reported here overlaps with the observed electron density. Although the only dockings involving hydrogen bonding of the cholesterol −OH group are those with the −OH group in the central pore, about a quarter of the 20 dockings returned by AutoDock Vina before selection based on hydrogen bonding showed the cholesterol molecule with its ring and −OH group, non-hydrogen bonded, within just the fenestration (Fig. 3 *D*). The fenestration is therefore wide enough to accommodate a cholesterol ring so that a cholesterol molecule could diffuse, −OH group first, from the central core of the lipid bilayer along the fenestration to reach the central pore. Epicholesterol (5-cholestan-3α-ol), in which the −OH group has a 3α rather than a 3β stereochemistry, has been shown to have a smaller effect than cholesterol on the function of many K^+ channels (31). Docking studies show that although epicholesterol can fit into the fenestrations of TWIK-1, the −OH group fails to make any hydrogen bonds with non-hydrogen-bonded atoms in the pore (data not shown).

In TWIK-1, the two openings to the bilayer interior, one on each side of the dimer, are symmetrical, and docking of cholesterol is observed equally in the two fenestrations. In contrast, in the two-pore domain TRAAK channel, in what is referred to as the down or nonconductive state, packing of the two monomers making up the channel is nonsymmetrical, with one of the two openings to the bilayer interior being much smaller than that in TWIK-1, whereas the other is much larger (32). In the alternative up or conductive state of the TRAAK channel, TM4 in one of the subunits moves to pack against TM2 of the other subunit, closing the larger of the two fenestrations (Fig. S3, *A* and *B*). Docking of cholesterol is only observed in the larger of the two fenestrations, and, indeed, the size of the fenestration is such that a cholesterol molecule can be docked either way round, with the cholesterol-OH hydrogen bonding to either Ile127, Leu236, Thr237, or Thr238 in the central cavity or to Leu151 on the outer surface (Fig. S3, *C* and *D*; Table S2). In all these binding modes, the cholesterol molecule is located under the selectivity filter and so could block ion movement through the channel. In the up or conductive state, no docking of cholesterol is observed in the fenestrations (Table S2). In both the up and down states of TRAAK, docking is also observed to the outer surface of the channel, to Tyr42, or to the neighboring Ser45 (Table S2).

The fenestrations in TREK-2 are similar to those in TRAAK, and, as in TRAAK, the fenestrations are closed off by movement of TM4 in the up state (28); in this state, cholesterol binds only to Tyr87 on the protein surface and does not occupy the fenestrations (Table S2). In contrast, in the down state, cholesterol binds in the fenestration, hydrogen bonding to Leu279 or Thr281 in pore helix 2, to Ile170 in pore helix 1, or to Ile194 in TM2 (Table S2). Prozac (fluoxetine) binds in the fenestrations of TREK-2 in a binding site defined by Ile194, Leu279, and Thr280 (28) so that binding of Prozac and cholesterol will be competitive. The only available structures for TREK-1 are in the up state with no large, open fenestrations, and the only binding observed is to the protein surface, to residues in TM1, TM3, or TM4 (Table S2).

In the Kv family of four subunit K^+ channels, binding of cholesterol is observed to either a single site on the channel surface or to no sites (Table S2). For the homotetrameric Kir family, no binding is observed to the channel surface, but binding is seen in the central cavity of the channel, the cholesterol hydrogen bonding to either Gln141 in the pore helix or to Trp94 in TM1 (Table S2). However, unlike the two-pore K^+ channels, Kir channels contain no fenestrations that would allow direct entry of cholesterol molecules from the surrounding lipid bilayer into the channel. The G-protein-gated K^+ channel GIRK2 is also homotetrameric, with a structure similar to that of Kir2.2 (33,34), and again a cholesterol molecule binds in the central pore just below the selectivity filter, hydrogen bonding to Ser181 in TM2; in the constitutionally active R201A mutant in the presence of phosphatidylinositol 4,5-bisphosphate (PIP_2), four strong binding modes are observed in the central cavity, with hydrogen bonding to Tyr102 in TM1, Ser181 and Ser177 in TM2, and Glu152 in the pore helix. GIRK2, like Kir2.2, lacks any fenestrations.

In the tetrameric transient receptor potential channel family, cholesterol molecules bind to the protein surface, generally to a residue in the deep clefts between subunits such as Thr550 in TRPV1, Tyr439 and Ser503 in TRPML1, Tyr491 in TRPML3, and Thr663 and Tyr611 in PKD2, but these bound cholesterol molecules do not penetrate into the central pore (Table S2). Thr550 in TRPV1 has been shown to hydrogen bond to the ligand homovanillyl ester, whose binding site is also occupied by phosphatidylinositols (35). Similarly, in the GluA2 glutamate receptor family, cholesterol molecules bind in the clefts between subunits but do not penetrate into the central cavity to block the channel.

In the closed apo or antagonist-bound state of the trimeric ATP-gated P2X3 channel, binding of cholesterol is only seen to Thr336 or Ser36 on the external surface (Table S2). However, in the open channel, Thr336 becomes occluded by a neighboring subunit, and Thr330, previously occluded, now hydrogen bonds to a cholesterol molecule with its −OH group in the central cavity and its chain in the very large fenestrations or lateral portals that link the channel pore to the core of the lipid bilayer (Fig. 4); Thr330 is located at the narrowest region of the pore gate

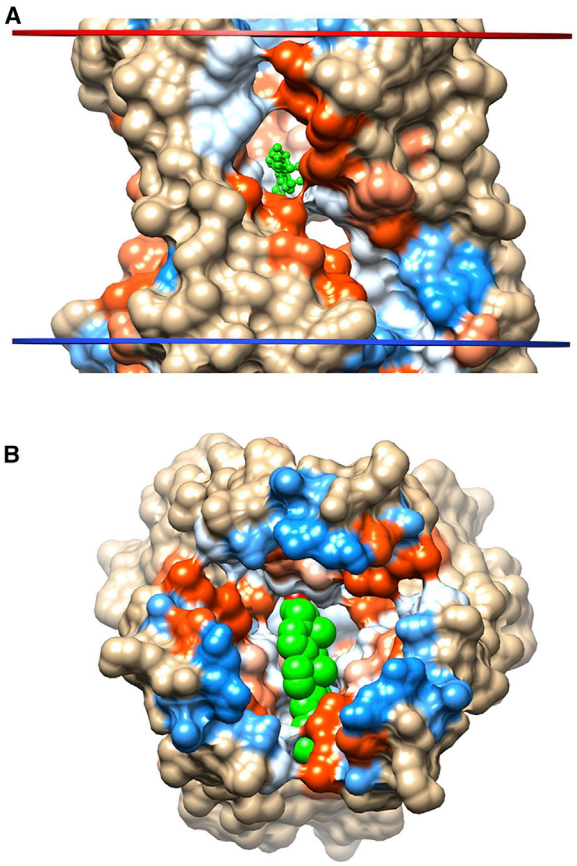

FIGURE 4 Cholesterol binding within the central pore of the open-state homotrimeric ATP-gated P2X3 channel (PDB: 5SVK). (*A*) The TM surface showing the large portals connecting the channel pore to the central core of the lipid bilayer is shown with a bound cholesterol (*green*). (*B*) A view of the TM domain from the EC side with the EC domains removed shows a cholesterol (*spheres*) bound in the channel pore. To see this figure in color, go online.

on the cytoplasmic side (36). Ions are suggested to enter the transmembrane pore via the lateral portals (36,37); a cholesterol molecule bound to Thr330 might not completely block the portal because of the large size of the portal (Fig. 4 *A*). The structure of the channel in the desensitized state is more like that in the open state than that in the closed state (36), and cholesterol again binds to Thr330 and the adjacent Ser331. Very similar results are observed for the P2X4 channel, with cholesterol binding to the non-hydrogen-bonded carbonyls of Gly343 (in PDB: 4DW1) or Ala 344 (in PDB: 5WZY) at the pore constriction in the open channel, with no binding in the closed channel. In the open-channel form of the P2X4 channel of the Golf Coast tick, no binding is observed in the open channel, as the carbonyl group of the residue at the pore constriction, Val361, is hydrogen bonded within helix TM2 (38). For the P2X7 channel bound to the competitive antagonist TNP-ATP, the channel is in an expanded, incompletely activated conformation (39), and cholesterol does not bind in the pore but to −OH containing residues exposed on the protein surface (Table S2). The acid-sensing ion channel adopts a structure very similar to those of the P2X channels (40), and the closed form of the acid-sensing ion channel shows no binding of cholesterol either in the pore or to surface exposed sites.

G-protein-coupled receptors

Docking was performed for 146 class A GPCR structures, representing 36 different members of the class A family, with cholesterol binding observed to 60% of them (Table S1). The frequencies with which the seven TM α-helices of the receptors provided residues acting as proton donors or acceptors to deep cholesterol molecules are all rather similar, but with TM5 having the highest probability of containing such residues (Fig. S4). In a few cases, the same residues appear in docking sites in more than two members of the family, particularly noticeable for residues at positions 5.46/5.461 and 7.47 in the Ballesteros-Weinstein numbering system (Table S5) (41).

For the 5-hydroxytrytamine 5-HT_{1B} receptor, a cholesterol-binding site was detected involving the side chain of Thr64 in TM1 and the backbone oxygen of Ser99 in TM2, which is not hydrogen bonded in the helix because of the presence of Pro104 (Table S1); Ser99, but not Thr64, is conserved in the 5-HT_{1A} receptor. The level of binding of 5-HT to the 5-HT_{1A} receptor decreases on removal of cholesterol and is restored by the readdition of either cholesterol or *ent*-cholesterol, the mirror image of cholesterol, but not by epicholesterol (42). Docking studies with the 5-HT_{1B} receptor and *ent*-cholesterol give the same results as for cholesterol, whereas docking with epicholesterol returned no binding sites (data not shown), leaving open the possibility of a functional role for binding of cholesterol to Ser99. For the 5-HT_{2B} receptor, two cholesterol-binding sites were detected, one involving the side chain of Thr228 in TM5 and the other involving the backbone oxygen of Met63 in TM1 (Table S1). Thr228 is adjacent to the Pro-Ile-Phe motif that forms an interface between TM3, TM5, and TM6 near the base of the ligand binding pocket (43), and mutation of Thr228 to Ala resulted in a very large reduction in affinity for 5-HT (44).

Thirty structures are available for the A_{2A} adenosine receptor with resolutions of 3.5 Å or better, and of these, 18 showed no binding sites for cholesterol in the docking analysis (Table S1). One structure (PDB: 3UZA) showed binding to the backbone oxygen of Cys185 in TM5. Although the presence of Pro189 in TM5 results in the backbone oxygen of Cys185 not forming a hydrogen bond within TM5, in all the crystal structures except for 3UZA, this backbone oxygen is hydrogen bonded to the side chain of Gln89 in TM3. The remaining 11 structures showed binding to a pair of residues, Gly56 and Val57, in TM2 with binding energies between −6.1 and −5.5 kcals mol^{-1} (Table S1). There are small differences in the locations of the backbone oxygens of Gly56 and Val57 and in the surface pockets

reported by CASTp between structures that do and do not show binding sites for cholesterol (Fig. S5). Some of these differences in surface pockets could be due to the presence of thermostabilizing mutations in some structures, the most common of which are the StarR2 set of eight mutations, one of which, Leu54, is close to the Gly56/Val57 pair. Small differences could also arise from the variety of insertions used to aid crystallization and from the different agonists and antagonists included in the crystallization media or could be a result of the relatively low resolutions of some of the structures.

The β_2 adrenergic receptor shows cholesterol binding to both the inactive and active states but to different sites (Fig. 2; Table 1), suggesting that binding of cholesterol could result in a shift in equilibrium between the different conformational states of the receptor. The presence of cholesterol results in an increase in affinity for the partial inverse agonist timolol but not for the full agonist isoproterenol (3). Mutation of Gly320 in TM7, part of one of the binding sites in the inactive state, resulted in a halving of the affinity for isoproterenol, and the sequence NPLIY in TM7, containing the Pro residue responsible for the backbone oxygen of Gly320 not being hydrogen bonded, is conserved in the β_2 adrenergic receptor family (45,46). Mutation of Glu122, part of the binding site in the active receptor (Table 1), led to reduced affinity for both agonists and antagonists, and Glu122 has been suggested to be part of a pathway linking allosteric changes on the two sides of the receptor (47,48). Cholesterol-binding sites are also detected on the muscarinic acetylcholine receptor family, and the presence of cholesterol has been shown to result in a large increase in the affinity of the M1 receptor for the antagonist quinuclidinylbenzylate (49).

The results for bovine rhodopsin and opsin are very different from those for most class A GPCRs in that of the 20 high resolution structures, only one (PDB: 3CAP) shows cholesterol binding (Table S1). In the 3CAP structure, both atoms of the −OH group of Thr297 are non-hydrogen bonded and exposed on the protein surface and interact with a deep cholesterol molecule, whereas in all the other structures, a simple rotation of the Thr297 side chain about the C_A-C_B bond results in the −OH group being hydrogen bonded either to the backbone O of Phe294 in rhodopsin or to the backbone O of Phe293 in opsin. In mammals, rhodopsin is located in disks formed by invagination of the plasma membrane so that newly formed disk membranes are rich in cholesterol, whereas the cholesterol content of older disks has fallen from the original 30 mol% to approximately 5 mol% (50). In contrast, in squid, rhodopsin is located in cholesterol-rich microvilli (51), and as shown in Table S1, strong hydrogen bonding of cholesterol to Leu85 is observed in TM2.

Mutational studies in other classes of GPCR are also consistent with an important role for some of the residues identified as being involved in cholesterol binding (Table S1). In two class B GPCRs, the corticotrophin-releasing factor receptor 1 and the glucagon receptor, interaction of cholesterol is observed with the side-chain −OH of a Thr or Ser residue at positions 2.62 or 2.63 in the numbering system of Wootten et al. (52). Mutation of Ser189$^{2.62}$ in the human glucagon receptor led to a small increase in the affinity for glucagon, whereas mutation of the adjacent Val191$^{2.64}$ lead to a large decrease in affinity (53). In the class C metabotropic glutamate receptor, interaction of cholesterol is observed with Ser715 and Thr719 in TM4, and mutation of either of these residues has been shown to lead to a reduced affinity for glutamate (54).

Transporters

Cholesterol binding to the Ca^{2+}-ATPase of muscle sarcoplasmic reticulum is complex, with different patterns of binding for the different conformational states of the protein (Table S3). For a wide variety of Ca^{2+}-bound forms, binding is observed to some or all of Ser942 (TM9), Leu797 (TM6), and Thr906/Met909 (TM8) with no binding to these residues in non-Ca^{2+}-bound forms, reflecting changes in helix packing on binding Ca^{2+}. Binding of thapsigargin favors the E2 conformation of the Ca^{2+}-ATPase, and cholesterol binds to thapsigargin-bound forms predominantly at Cys268/Tyr295, again reflecting changes in helix packing. The Na^+,K^+-ATPase also shows a complex pattern of binding, with distinct differences between phosphorylated and nonphosphorylated forms (Table S3).

The solute carrier transporter superfamily member Glut1 in inhibitor-bound forms of the inward-open state shows binding of cholesterol to the side chain of Ser73 located at the bottom of a large hole forming part of the domain-domain interface between TM2 and TM11 (Table S3); in the inhibitor-free structure, the Ser73 side chain points into the central cavity, and no binding of cholesterol is observed. Binding to the external surface is also observed for the Glut5 fructose transporter in the open-outward form to Ser422 in cow and its equivalent Ser421 in rat, and in the open-inward form, binding is also observed to Thr452 and Thr354 (Table S3). In the mitochondrial ADP/ATP carrier, cholesterol binds to Gly224 or Arg234 in the large central cavity where the inhibitor carboxyatractyloside also binds (Table S3). Although the cholesterol content of mitochondria is generally very low, in hepatoma cells, it can increase to approximately 20 mol% in the inner mitochondrial membrane, and in reconstituted systems, high levels of cholesterol inhibit the rate of transport of ATP by the ADP/ATP carrier (55).

The P-glycoprotein, a member of the ABC transporter family, consists of two pseudosymmetric halves encoded in a single polypeptide chain. In the nucleotide-free, inward-facing state, cholesterol binds to either His60 or Tyr303, spanning the central cavity of the protein (Fig. 5 *A*), and to Thr765 on the membrane-exposed surface (Table S3). In

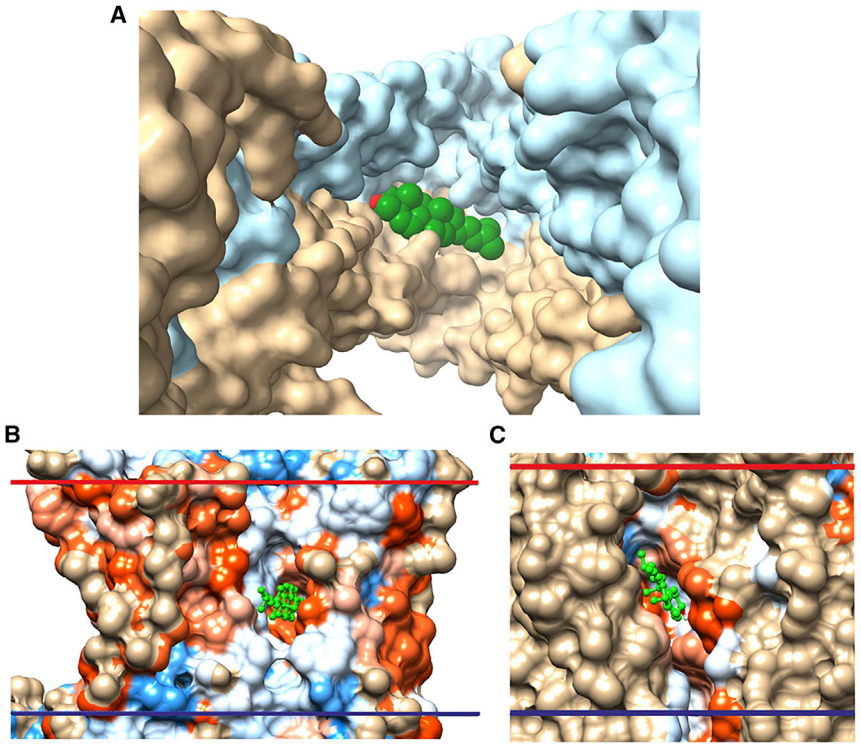

FIGURE 5 Binding of cholesterol to P-glycoprotein and two mitochondrial complexes. (*A*) A view of the P-glycoprotein (PDB: 4Q9H) from the IC side shows a bound cholesterol (*green*), with the two domains colored blue and tan. (*B* and *C*) TM surfaces of cytochrome bc1 (PDB: 1BGY) and cytochrome c oxidase (PDB: 1V54), respectively, are given, showing lipid-exposed pockets with bound cholesterol molecules. To see this figure in color, go online.

the nucleotide-bound, outward-facing state, cholesterol no longer binds in the central cavity, although binding in the central cavity is observed in the nucleotide-bound, outward-facing state of the MRP-1 drug resistance protein (Table S3). The P-glycoprotein has been reported to transport cholesterol across the membrane, and the function of the P-glycoprotein is modified by cholesterol in the membrane (56,57). The ABCB10 mitochondrial ABC transporter is a homodimer, and although cholesterol binds in the central cavity, most binding modes involve solely one or other of the two monomers, and only rarely does a cholesterol molecule span between the two halves; Ser181, one of the identified hydrogen bond partners, has been suggested to be part of a conserved binding site for amphipathic substrates (58). For the cystic fibrosis transmembrane conductance regulator, binding is observed to the outer face of the transporter and to the inner cavity, but again with no bridging between the two halves of the cavity (Table S3).

Other classes of membrane protein

Results for other classes of membrane protein are listed in Table S4. Most show binding of cholesterol to the membrane-exposed surfaces of the protein. However, for the CAAX intramembrane proteases, binding is limited to the large central hydrophobic cavity. In the electron transport chain complex II, binding is to the external surface of the complex, whereas in complex III (Cytochrome bc1), binding is observed to Tyr358 in subunit C in a large cleft open to the hydrophobic core of the lipid bilayer (Fig. 5 *B*). In electron transport chain complex IV (cytochrome c oxidase), binding is similarly observed to Ser89 at the bottom of a deep lipid-exposed cleft (Fig. 5 *C*) as well as to other residues on the lipid-exposed surface of the complex.

CONCLUSIONS

It is shown here that Autodock Vina can be used, with modified binding parameters, to study protein binding of cholesterol molecules deep in the membrane. Errors in docking studies are generally calculated based on root mean-square deviation between a crystallographically determined bound ligand structure at some site and the structure of a ligand docked to that site. Estimating error in this way is not possible for the deep cholesterol binding sites, as there are no crystallographic data, and root mean-square deviation cannot be measured between an atomic structure (for cholesterol in docking studies) and a coarse-grained structure (cholesterol in CGMD simulations). However, the fact that the hydrogen-bond partners identified here by docking match those present at binding sites identified by CGMD simulation, with no false hits, suggest that the reliability of docking is high.

The studies reported here detect binding of deep cholesterol molecules to 60% of the 146 GPCR structures studied, including examples in which binding differs between the active and inactive states of the receptor. Binding is observed in the fenestrations of two-pore K^+ channels,

with the cholesterol chain in a fenestration and the cholesterol −OH and ring in the central pore, where it can block ion flow through the channel; in the TRAAK channel, binding is only observed for the nonconductive state and not for the conductive state. Conformation-specific binding is also observed in the fenestrations of the trimeric ATP-gated P2X3 channels; for a number of transporters, including Glut1, Glut5, and P-glycoprotein; and in mitochondrial complexes. These studies demonstrate the importance of the many non-hydrogen-bonded atoms exposed on the TM surfaces or in central cavities in many membrane proteins provided by the polypeptide backbone in proline-containing TM helices and by residue side chains. It is suggested that interaction between these proton donors and acceptors and molecules of cholesterol could be functionally important, the probability of a binding event being high even though only a small proportion of the cholesterol molecules in a membrane are located deep within the membrane core, because of the strength of a hydrogen bond formed in a hydrophobic environment.

Tables S1–S4 give all current predicted cholesterol binding sites. These data are also available and will be updated at the DeepCholesterol web site (https://deepcholesterol.soton.ac.uk).

SUPPORTING MATERIAL

Five figures and five tables are available at http://www.biophysj.org/biophysj/supplemental/S0006-3495(18)30727-6.

ACKNOWLEDGMENTS

The Centre for Biological Sciences, University of Southampton is thanked for computing facilities.

SUPPORTING CITATIONS

References (59,60) appear in the Supporting Material.

REFERENCES

1. Genheden, S., J. W. Essex, and A. G. Lee. 2017. G protein coupled receptor interactions with cholesterol deep in the membrane. *Biochim. Biophys. Acta.* 1859:268–281.
2. Feldblum, E. S., and I. T. Arkin. 2014. Strength of a bifurcated H bond. *Proc. Natl. Acad. Sci. USA.* 111:4085–4090.
3. Hanson, M. A., V. Cherezov, …, R. C. Stevens. 2008. A specific cholesterol binding site is established by the 2.8 A structure of the human β_2-adrenergic receptor. *Structure.* 16:897–905.
4. Song, Y., A. K. Kenworthy, and C. R. Sanders. 2014. Cholesterol as a co-solvent and a ligand for membrane proteins. *Protein Sci.* 23:1–22.
5. Fantini, J., and F. J. Barrantes. 2013. How cholesterol interacts with membrane proteins: an exploration of cholesterol-binding sites including CRAC, CARC, and tilted domains. *Front. Physiol.* 4:31.
6. Hedger, G., and M. S. P. Sansom. 2016. Lipid interaction sites on channels, transporters and receptors: recent insights from molecular dynamics simulations. *Biochim. Biophys. Acta.* 1858:2390–2400.
7. Zhang, K., J. Zhang, …, Q. Zhao. 2014. Structure of the human P2Y12 receptor in complex with an antithrombotic drug. *Nature.* 509:115–118.
8. Gimpl, G. 2016. Interaction of G protein coupled receptors and cholesterol. *Chem. Phys. Lipids.* 199:61–73.
9. Marquardt, D., N. Kučerka, …, J. Katsaras. 2016. Cholesterol's location in lipid bilayers. *Chem. Phys. Lipids.* 199:17–25.
10. Marquardt, D., F. A. Heberle, …, J. Katsaras. 2016. Lipid bilayer thickness determines cholesterol's location in model membranes. *Soft Matter.* 12:9417–9428.
11. Marrink, S. J., A. H. de Vries, …, S. R. Wassall. 2008. Cholesterol shows preference for the interior of polyunsaturated lipid membranes. *J. Am. Chem. Soc.* 130:10–11.
12. Prasanna, X., A. Chattopadhyay, and D. Sengupta. 2014. Cholesterol modulates the dimer interface of the β_2-adrenergic receptor via cholesterol occupancy sites. *Biophys. J.* 106:1290–1300.
13. Ingólfsson, H. I., T. S. Carpenter, …, F. C. Lightstone. 2017. Computational lipidomics of the neuronal plasma membrane. *Biophys. J.* 113:2271–2280.
14. Ben-Tal, N., D. Sitkoff, …, B. Honig. 1997. Free energy of amide hydrogen bond formation in vacuum, in water, and in liquid alkane solution. *J. Phys. Chem. B.* 101:450–457.
15. Trott, O., and A. J. Olson. 2010. AutoDock Vina: improving the speed and accuracy of docking with a new scoring function, efficient optimization, and multithreading. *J. Comput. Chem.* 31:455–461.
16. Ross, G. A., G. M. Morris, and P. C. Biggin. 2012. Rapid and accurate prediction and scoring of water molecules in protein binding sites. *PLoS One.* 7:e32036.
17. Lomize, A. L., I. D. Pogozheva, …, H. I. Mosberg. 2006. Positioning of proteins in membranes: a computational approach. *Protein Sci.* 15:1318–1333.
18. Pettersen, E. F., T. D. Goddard, …, T. E. Ferrin. 2004. UCSF Chimera–a visualization system for exploratory research and analysis. *J. Comput. Chem.* 25:1605–1612.
19. Morris, G. M., R. Huey, …, A. J. Olson. 2009. AutoDock4 and AutoDockTools4: automated docking with selective receptor flexibility. *J. Comput. Chem.* 30:2785–2791.
20. Binkowsk, T. A., S. Naghibzadeh, and J. Liang. 2003. CASTp: computed atlas of surface topography of proteins. *Nucleic Acids Res.* 31:3352–3355.
21. Luxnat, M., and H. J. Galla. 1986. Partition of chlorpromazine into lipid bilayer membranes: the effect of membrane structure and composition. *Biochim. Biophys. Acta.* 856:274–282.
22. Sankaram, M. B., and T. E. Thompson. 1990. Modulation of phospholipid acyl chain order by cholesterol. A solid-state ^{2}H nuclear magnetic resonance study. *Biochemistry.* 29:10676–10684.
23. Lee, A. G. 2004. How lipids affect the activities of integral membrane proteins. *Biochim. Biophys. Acta.* 1666:62–87.
24. Marrink, S. J., and D. P. Tieleman. 2013. Perspective on the Martini model. *Chem. Soc. Rev.* 42:6801–6822.
25. Javanainen, M., H. Martinez-Seara, and I. Vattulainen. 2017. Excessive aggregation of membrane proteins in the Martini model. *PLoS One.* 12:e0187936.
26. Miller, A. N., and S. B. Long. 2012. Crystal structure of the human two-pore domain potassium channel K2P1. *Science.* 335:432–436.
27. Brohawn, S. G., J. del Mármol, and R. MacKinnon. 2012. Crystal structure of the human K2P TRAAK, a lipid- and mechano-sensitive K^+ ion channel. *Science.* 335:436–441.
28. Dong, Y. Y., A. C. Pike, …, E. P. Carpenter. 2015. K2P channel gating mechanisms revealed by structures of TREK-2 and a complex with Prozac. *Science.* 347:1256–1259.
29. Lolicato, M., C. Arrigoni, …, D. L. Minor, Jr. 2017. K_{2P}2.1 (TREK-1)-activator complexes reveal a cryptic selectivity filter binding site. *Nature.* 547:364–368.

30. Aryal, P., F. Abd-Wahab, …, S. J. Tucker. 2015. Influence of lipids on the hydrophobic barrier within the pore of the TWIK-1 K2P channel. *Channels (Austin).* 9:44–49.

31. Levitan, I., D. Singh, and A. Rosenhouse-Dantsker. 2014. Cholesterol binding to ion channels. *Front. Physiol.* 5:65.

32. Brohawn, S. G., E. B. Campbell, and R. MacKinnon. 2014. Physical mechanism for gating and mechanosensitivity of the human TRAAK K^+ channel. *Nature.* 516:126–130.

33. Whorton, M. R., and R. MacKinnon. 2011. Crystal structure of the mammalian GIRK2 K^+ channel and gating regulation by G proteins, PIP_2, and sodium. *Cell.* 147:199–208.

34. Whorton, M. R., and R. MacKinnon. 2013. X-ray structure of the mammalian GIRK2-βγ G-protein complex. *Nature.* 498:190–197.

35. Gao, Y., E. Cao, …, Y. Cheng. 2016. TRPV1 structures in nanodiscs reveal mechanisms of ligand and lipid action. *Nature.* 534:347–351.

36. Mansoor, S. E., W. Lü, …, E. Gouaux. 2016. X-ray structures define human P2X(3) receptor gating cycle and antagonist action. *Nature.* 538:66–71.

37. Samways, D. S., Z. Li, and T. M. Egan. 2014. Principles and properties of ion flow in P2X receptors. *Front. Cell. Neurosci.* 8:6.

38. Kasuya, G., Y. Fujiwara, …, O. Nureki. 2016. Structural insights into divalent cation modulations of ATP-gated P2X receptor channels. *Cell Rep.* 14:932–944.

39. Kasuya, G., T. Yamaura, …, O. Nureki. 2017. Structural insights into the competitive inhibition of the ATP-gated P2X receptor channel. *Nat. Commun.* 8:876.

40. Gonzales, E. B., T. Kawate, and E. Gouaux. 2009. Pore architecture and ion sites in acid-sensing ion channels and P2X receptors. *Nature.* 460:599–604.

41. Ballesteros, J. A., and H. Weinstein. 1995. Integrated methods for the construction of three-dimensional models and computational probing of structre-function relations in G protein-coupled receptors. *In* Methods in Neurosciences C. S. Stuart, ed. . Academic Press, pp. 366–428.

42. Jafurulla, M., B. D. Rao, …, A. Chattopadhyay. 2014. Stereospecific requirement of cholesterol in the function of the serotonin1A receptor. *Biochim. Biophys. Acta.* 1838:158–163.

43. Wacker, D., C. Wang, …, R. C. Stevens. 2013. Structural features for functional selectivity at serotonin receptors. *Science.* 340:615–619.

44. Manivet, P., B. Schneider, …, J. M. Launay. 2002. The serotonin binding site of human and murine 5-HT2B receptors: molecular modeling and site-directed mutagenesis. *J. Biol. Chem.* 277:17170–17178.

45. Kikkawa, H., M. Isogaya, …, H. Kurose. 1998. The role of the seventh transmembrane region in high affinity binding of a β_2-selective agonist TA-2005. *Mol. Pharmacol.* 53:128–134.

46. Barak, L. S., L. Ménard, …, M. G. Caron. 1995. The conserved seven-transmembrane sequence $NP(X)_{2,3}Y$ of the G-protein-coupled receptor superfamily regulates multiple properties of the β_2-adrenergic receptor. *Biochemistry.* 34:15407–15414.

47. Ghanouni, P., H. Schambye, …, B. K. Kobilka. 2000. The effect of pH on beta(2) adrenoceptor function. Evidence for protonation-dependent activation. *J. Biol. Chem.* 275:3121–3127.

48. Bhattacharya, S., and N. Vaidehi. 2014. Differences in allosteric communication pipelines in the inactive and active states of a GPCR. *Biophys. J.* 107:422–434.

49. Berstein, G., T. Haga, and A. Ichiyama. 1989. Effect of the lipid environment on the differential affinity of purified cerebral and atrial muscarinic acetylcholine receptors for pirenzepine. *Mol. Pharmacol.* 36:601–607.

50. Albert, A., D. Alexander, and K. Boesze-Battaglia. 2016. Cholesterol in the rod outer segment: a complex role in a "simple" system. *Chem. Phys. Lipids.* 199:94–105.

51. Mason, W. T., and E. W. Abrahamson. 1974. Phase transitions in vertebrate and invertebrate photoreceptor membranes. *J. Membr. Biol.* 15:383–392.

52. Wootten, D., J. Simms, …, P. M. Sexton. 2013. Polar transmembrane interactions drive formation of ligand-specific and signal pathway-biased family B G protein-coupled receptor conformations. *Proc. Natl. Acad. Sci. USA.* 110:5211–5216.

53. Siu, F. Y., M. He, …, R. C. Stevens. 2013. Structure of the human glucagon class B G-protein-coupled receptor. *Nature.* 499:444–449.

54. Fukuda, J., G. Suzuki, …, H. Ohta. 2009. Identification of a novel transmembrane domain involved in the negative modulation of mGluR1 using a newly discovered allosteric mGluR1 antagonist, 3-cyclohexyl-5-fluoro-6-methyl-7-(2-morpholin-4-ylethoxy)-4H-chromen-4-one. *Neuropharmacology.* 57:438–445.

55. Woldegiorgis, G., and E. Shrago. 1985. Adenine nucleotide translocase activity and sensitivity to inhibitors in hepatomas. Comparison of the ADP/ATP carrier in mitochondria and in a purified reconstituted liposome system. *J. Biol. Chem.* 260:7585–7590.

56. Kimura, Y., N. Kioka, …, K. Ueda. 2007. Modulation of drug-stimulated ATPase activity of human MDR1/P-glycoprotein by cholesterol. *Biochem. J.* 401:597–605.

57. Clay, A. T., P. Lu, and F. J. Sharom. 2015. Interaction of the P-glycoprotein multidrug transporter with sterols. *Biochemistry.* 54:6586–6597.

58. Shintre, C. A., A. C. Pike, …, E. P. Carpenter. 2013. Structures of ABCB10, a human ATP-binding cassette transporter in apo- and nucleotide-bound states. *Proc. Natl. Acad. Sci. USA.* 110:9710–9715.

59. Pin, J. P., T. Galvez, and L. Prézeau. 2003. Evolution, structure, and activation mechanism of family 3/C G-protein-coupled receptors. *Pharmacol. Ther.* 98:325–354.

60. Wang, C., H. Wu, …, R. C. Stevens. 2014. Structural basis for Smoothened receptor modulation and chemoresistance to anticancer drugs. *Nat. Commun.* 5:4355.

Biophysical Journal, Volume *115*

Supplemental Information

A Database of Predicted Binding Sites for Cholesterol on Membrane Proteins, Deep in the Membrane

Anthony G. Lee

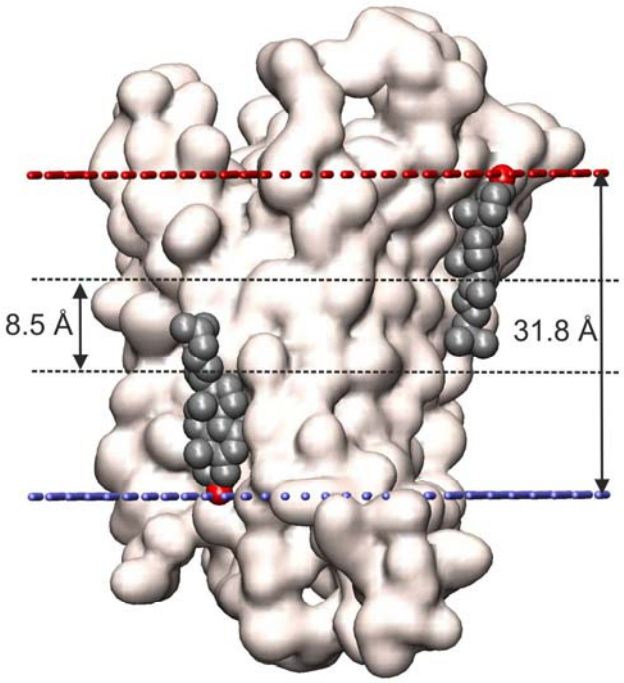

FIGURE S1 Cholesterol molecules in the crystal structure of human purinergic G protein coupled receptor $P2Y_{12}$. The protein surface (PDB code 4NTJ) is shown together with its hydrophobic domain of thickness 31.8 Å as predicted by the OPM database; the EC and IC surfaces are shown in red and blue, respectively. The two resolved cholesterol molecules are shown in space-fill format with oxygen atoms in red. The ends of the two cholesterol rings are separated by 8.5 Å.

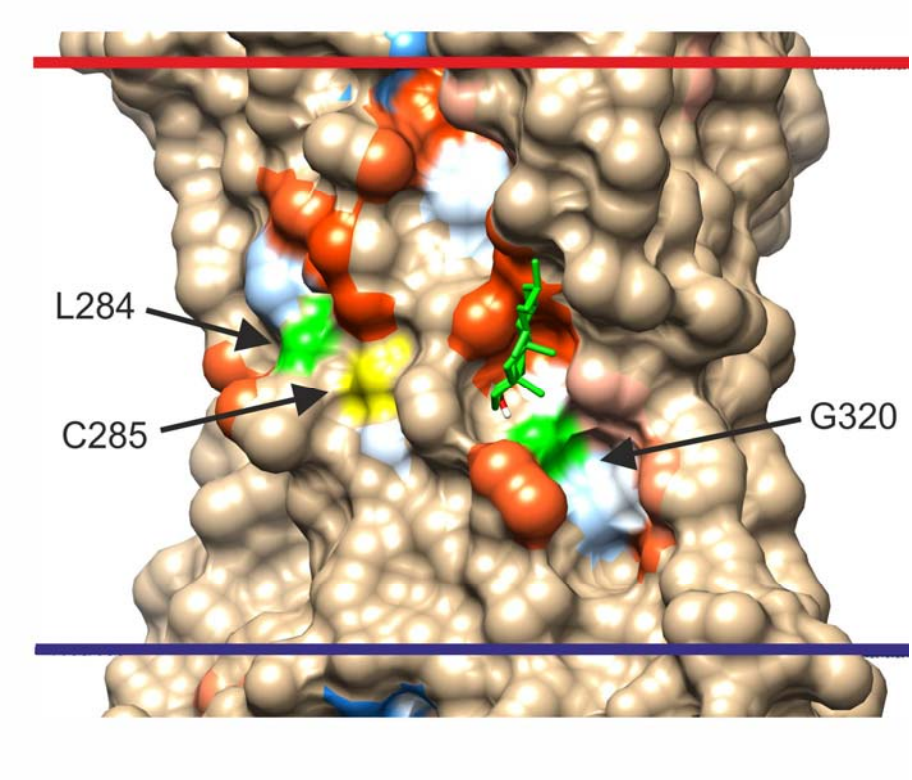

FIGURE S2 The membrane spanning surface of the agonist-free β_2 adrenergic receptor [PDB file 3D4S] with the surface pockets identified using CASTp, coloured from the most hydrophobic (orange) to the most hydrophilic (blue). The most energetically favourable of the cholesterol molecules bound to Gly320 is shown in stick format (light green for carbons and red for oxygen). The locations of the backbone oxygens of Gly320 and Leu284 are shown in green and the side chain S of Cys285 is shown in yellow. Gly320 is the only one of these residues located in a surface pocket.

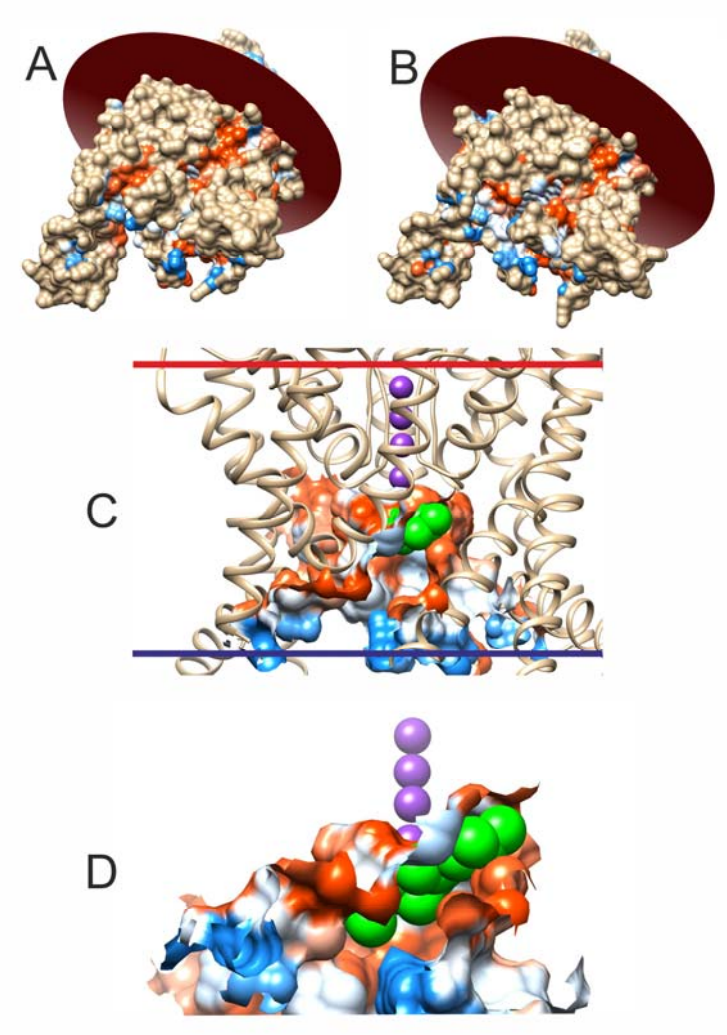

FIGURE S3 Cholesterol docking to TRAAK channels. (*A*, *B*) The membrane-spanning regions of the TRAAK channel in the up (*A*; PDF file 4WFE) and down states (*B*; PDF file 4WFF) with the EC membrane surface shown in red. The views are tilted to show the large openings on the IC side in both the up and down states and the fenestrations present in the down (*B*) but not up (*A*) states. (*C*, *D*) Two views of a bound cholesterol molecule (green) hydrogen bonded to Leu151 in the central cavity in the down state, just below the selectivity filter, shown occupied by four K^+ ions (purple).

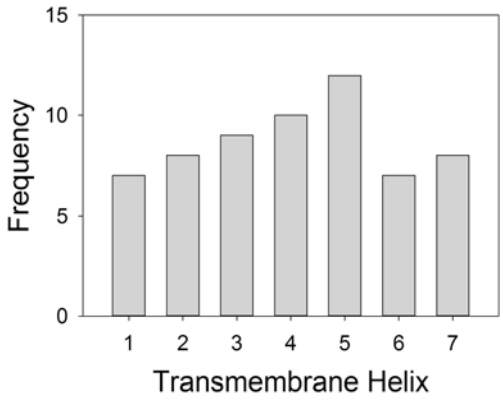

FIGURE S4 Helix involvement in deep cholesterol binding to A class GPCRs. The frequencies with which the seven TM α-helices in the 36 GPCRs studied provide residues involved in hydrogen bonding to deep cholesterol molecules.

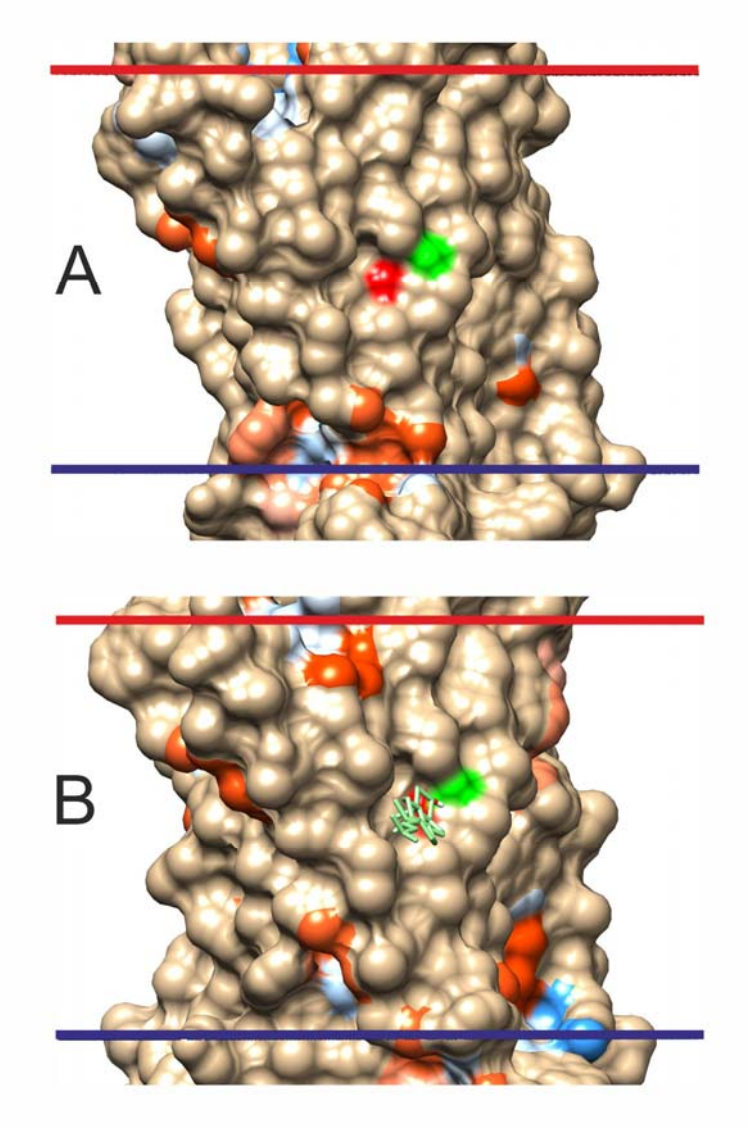

FIGURE S5 Cholesterol binding to the antagonist-bound A_{2A} adenosine receptor. The TM surfaces of PDB files 4EIY (*A*) and 5UIG (*B*) showing surface pockets identified using CASTp. The 5UIG structure shows a single binding site of binding energy -6.1 kcals mol^{-1}. The locations of the backbone oxygens of Gly56 and Val57 are coloured red and green respectively.

TABLE S1 GPCRs

E[1]	Donor	Acceptor			Local Residues (within 3 Å of a cholesterol –OH group)				
GPCR Class A[2]									
5-hydroxytryptamine receptor 1B,bound ergotamine, Human 4iar									
-6.5	Chl	OH	Thr64 [1.47]	OG1	Thr64 [1.47]	Ser99 [2.54]			
5-hydroxytryptamine receptor 1B, bound dihydroergotamine, Human 4iaq									
-6.3	Chl	OH	Ser99 [2.54]	O	Thr64 [1.47]	Ser99 [2.54]			
	Chl	OH	Thr64 [1.47]	OG1					
-6.2	Chl	OH	Thr64 [1.47]	OG1	Thr60 [1.43]	Leu61 [1.44]	Thr64 [1.47]		
-5.8	Chl	OH	Thr64 [1.47]	OG1	Thr60 [1.43]	Thr64 [1.47]	Ser99 [2.54]		
5-hydroxytryptamine receptor 2B, bound ergotamine, Human 4ib4									
-6.0	Chl	OH	Thr228 [5.49]	OG1	Leu223 [5.45]	Phe227 [5.48]	Thr228 [5.49]		
-5.9	Chl	OH	Ala224 [5.46]	O	Ala224 [5.46]	Thr228 [5.49]			
	Chl	OH	Thr228 [5.49]	OG1	Ala224 [5.46]	Thr228 [5.49]			
-5.5	Chl	OH	Met63 [1.411]	O	Met63 [1.411]				
5-hydroxytryptamine receptor 2B, Human 4nc3									
-6.7	Chl	OH	Thr228 [5.49]	OG1	Ala224 [5.46]	Thr228 [5.49]			
-5.7	Chl	OH	Met63 [1.411]	O	Met63 [1.411]				
5-hydroxytryptamine receptor 2B, bound LSD, Human 5tvn									
-5.5	Chl	OH	Thr228 [5.49]	OG1	Thr228 [5.49]				
Adenosine receptor A1, Human 5uen									
-5.8	Ser246 [6.47]	OG	Chl	O	Leu242 [6.43]	Ser246 [6.47]			
Adenosine receptor A1 with PSB36 [PDB residues renumbered], Human 5n2s									
-5.8	Chl	OH	Ser246 [6.47]	OG	Ser246 [6.47]	Leu276 [7.40]	Asn280 [7.45]	Met283 [7.48]	
Adenosine receptor A2a, thermostable mutant, active-like, complex with agonist, Human 4uhr									
None									
Adenosine receptor A2a, thermostable mutant staR2, complex with antagonist, Human 3uza									
-5.8	Chl	OH	Cys185 [5.461]	O	Gln89 [3.37]	Cys185 [5.461]			
Adenosine receptor A2a, complex with inverse-agonist antibody and antagonist ZM241385, Human 3vg9									
-5.9	Chl	OH	Gly56 [2.54]	O	Gly56 [2.54]	Val57 [2.55]			
	Chl	OH	Val57 [2.55]	O					
Adenosine receptor A2a, complex with antagonist ZM241385, Human 3vga									
None									
Adenosine receptor A2a, inactive state, with antagonist ZM241385, Human 3eml									
None									
Adenosine receptor A2a, thermostable mutant staR2, complex with caffeine, Human 3rfm									
None									
Adenosine receptor A2a, thermostable mutant staR2, inactive state, complex with XAC, Human 3rey									
None									
Adenosine receptor A2a, thermostable mutant staR2, nactive state, with ZM241385, Human 3pwh									
None									

E^1	Donor	Acceptor	Local Residues (within 3 Å of a cholesterol –OH group)						
Adenosine receptor A2a, inactive state, with lipids and ZM241385, Human 4eiy									
None									
Adenosine receptor A2a, inactive state, with bound antagonist theophylline, Human 5k2a									
None									
Adenosine receptor A2a, inactive state, with bound antagonist theophylline, Human 5k2b									
None									
Adenosine receptor A2a, inactive state, with bound antagonist theophylline, Human 5k2c									
None									
Adenosine receptor A2a, inactive state, with bound antagonist theophylline, Human 5k2d									
None									
Adenosine receptor A2a, thermostable mutant staR2, inactive state, with bound antagonist theophylline, Human 5mzj									
-5.7	Chl	OH	Gly56 [2.54]	O	Gly56 [2.54]	Val57 [2.55]			
	Chl	OH	Val57 [2.55]	O					
Adenosine receptor A2a, thermostable mutant staR2, inactive state, with bound antagonist caffeine, Human 5mzp									
-5.6	Chl	OH	Gly56 [2.54]	O	Gly56 [2.54]	Val57 [2.55]			
	Chl	OH	Val57 [2.55]	O					
Adenosine receptor A2a, thermostable mutant staR2, inactive state, with bound antagonist PSB36, Human 5n2r									
None									
Adenosine receptor A2a,thermostable mutant staR2, inactive state, with bound antagonist ZMA, Human 5nlx									
None									
Adenosine receptor A2a, thermostable mutant staR2, inactive state, with bound antagonist ZMA, Human 5nm2									
None									
Adenosine receptor A2a,thermostable mutant staR2, inactive state, with bound antagonist ZMA, Human 5nm4									
None									
Adenosine receptor A2a,partially active state with agonist UK-432097, Human 3qak									
None									
Adenosine receptor A2a, thermostable mutant, partially active state with bound adenosine, Human 2ydo									
None									
Adenosine receptor A2a, thermostable mutant,partially active state with agonist NECA, Human 2ydv									
-5.5	Chl	OH	Gly56 [2.54]	O	Gly56 [2.54]	Val57 [2.55]			
	Chl	OH	Val57 [2.55]	O					
Adenosine receptor A2a, with G-alpha-S protein, Human 5g53									
None									
Adenosine receptor A2a, with triazole-carboximidamide antagonist, Human 5uig									
-6.1	Chl	OH	Gly56 [2.54]	O	Ala17 [1.43]	Gly56 [2.54]	Val57 [2.55]		
	Chl	OH	Val57 [2.55]	O					
Adenosine receptor A2a,thermostable mutant, with antagonist, Human 6aqf									
-5.5	Chl	OH	Val57 [2.55]	O	Gly56 [2.54]	Val57 [2.55]			
Adenosine receptor A2a, thermostable mutant StaR2, inactive with lipid, Human 5o1g									
-5.8	Chl	OH	Thr279 [7.44]	OG1	Val275 [7.40]	Leu276 [7.41]	Thr279 [7.44]		
-5.6	Chl	OH	Gly56 [2.54]	O	Gly56 [2.54]	Val57 [2.55]	Pro61 [2.59]		

E[1]	Donor		Acceptor		Local Residues (within 3 Å of a cholesterol –OH group)				
Adenosine receptor A2a, thermostable mutant StaR2, inactive with lipid, Human 5o1h									
-5.8	Chl	OH	Gly56 [2.54]	O	Gly56 [2.54]	Val57 [2.55]	Pro61 [2.59]		
-5.7	Chl	OH	Thr279 [7.44]	OG1	Val275 [7.40]	Leu276 [7.41]	Thr279 [7.44]		
	Chl	OH	Val57 [2.55]						
Adenosine receptor A2a, thermostable mutant StaR2, inactive with lipid, Human 5om1									
-5.7	Chl	OH	Gly56 [2.54]	O	Gly56 [2.54]	Val57 [2.55]			
	Chl	OH	Val57 [2.55]						
Adenosine receptor A2a, thermostable mutant StaR2, inactive with lipid, Human 5om4									
-5.7	Chl	OH	Gly56 [2.54]	O	Gly56 [2.54]	Val57 [2.55]			
	Chl	OH	Val57 [2.55]	O					
Adenosine receptor A2a, mylar structure, Human 5vra									
-6.0	Chl	OH	Gly56 [2.54]	O	Gly56 [2.54]	Val57 [2.55]			
	Chl	OH	Val57 [2.55]	O					

Angiotensin II receptor Type-1 (AT1) with bound antagonist, Human 4yay									
-5.6	Chl	OH	Phe251 [6.46]	O	Phe251 [6.46]				
Angiotensin II receptor Type-1 (AT1) with bound inverse agonist olmesartan, Human 4zud									
-6.8	Chl	OH	Ser252 [6.47]	OG	Phe248 [6.43]	Phe251 [6.46]	Ser252 [6.47]		
Angiotensin II receptor Type-2 (AT2) active-like state, Human 5ung									
-6.6	Chl	OH	Ser174 [4.56]	OG	Met170 [4.52]	Leu173 [4.55]	Ser174 [4.56]		
Angiotensin II receptor Type-2 (AT2) active-like state, Human 5unf									
-7.1	Chl	OH	Ser174 [4.56]	OG	Met170 [4.52]	Ser174 [4.56]			
Angiotensin II receptor Type-2 (AT2) active-like state, Human 5unh									
-6.6	Chl	OH	Ser174 [4.56]	OG	Met170 [4.52]	Leu173 [4.55]	Ser174 [4.56]		

Beta-1 adrenergic receptor with bound dobutamine, Turkey 2y00									
-6.1	Chl	OH	Ile214 [5.45]	O	Glu130 [3.41]	Ile214 [5.45]	Pro219 [5.50]		
Beta-1 adrenergic receptor with bound dobutamine, Turkey 2y01									
-6.7	Chl	OH	Leu171 [4.55]	O	Ala170 [4.54]	Leu171 [4.55]	Leu175 [4.59]		
-6.3	Chl	OH	Leu171 [4.55]	O	Ala170 [4.54]	Leu171 [4.55]	Phe174 [4.58]	Leu175 [4.59]	
-5.6	Chl	OH	Ile214 [5.45]	O	Glu130 [3.41]	Ile214 [5.45]	Pro219 [5.50]		
Beta-1 adrenergic receptor with bound carmoterol, Turkey 2y02									
-6.7	Chl	OH	Leu171 [4.55]	O	Ala170 [4.54]	Leu171 [4.55]	Leu175 [4.59]		
-6.3	Chl	OH	Leu171 [4.55]	O	Ala170 [4.54]	Leu171 [4.55]	Phe174 [4.58]	Leu175 [4.59]	
-5.8	Chl	OH	Ile214 [5.45]	O	Glu130 [3.41]	Ile214 [5.45]			
-5.5	Chl	OH	Glu130 [3.41]	OE2	Glu130 [3.41]	Ile214 [5.45]	Pro219 [5.50]		
	Chl	OH	Ile214 [5.45]	O					
Beta-1 adrenergic receptor with bound isoprenaline, Turkey 2y03									
-5.7	Chl	OH	Glu130 [3.41]	OE2	Glu130 [3.41]	Ile214 [5.45]			
	Chl	OH	Ile214 [5.45]	O					
Beta-1 adrenergic receptor with bound salbutamol, Turkey 2y04									
-5.9	Chl	OH	Ile214 [5.45]	O	Glu130 [3.41]	Ile214 [5.45]			
-5.8	Chl	OH	Leu171 [4.55]	O	Ala170 [4.54]	Leu175 [4.59]			

E[1]	Donor		Acceptor		Local Residues (within 3 Å of a cholesterol –OH group)				
Beta-1 adrenergic receptor, with bound carazolol, Turkey 2ycw									
-5.6	Chl	OH	Glu130 [3.41]	OE2	Glu130 [3.41]	Ile214 [5.45]			
	Chl	OH	Ile214 [5.45]	O					
Beta-1 adrenergic receptor, with bound cyanopindolol, Turkey 2ycx									
-5.7	Chl	OH	Glu130 [3.41]	OE2	Glu130 [3.41]	Ile214 [5.45]			
	Chl	OH	Ile214 [5.45]	O					
Beta-1 adrenergic receptor, with bound cyanopindolol, Turkey 2ycy									
None									
Beta-1 adrenergic receptor, with bound iodoctanopindolol, Turkey 2ycz									
-5.8	Chl	OH	Glu130 [3.41]	OE2	Glu130 [3.41]	Ile214 [5.45]			
	Chl	OH	Ile214 [5.45]	O					
-5.6	Chl	OH	Ile214 [5.45]	O	Glu130 [3.41]	Ile214 [5.45]	Pro219 [5.50]		
Beta-1 adrenergic receptor, basal state, Turkey 4gpo									
-5.5	Chl	OH	Glu130 [3.41]	OE2	Glu130 [3.41]	Ile214 [5.45]			
	Chl	OH	Ile214 [5.45]	O					
Beta-1 adrenergic receptor, inactive, engineered, Turkey 2vt4									
-5.8	Chl	OH	Ile214 [5.45]	O	Glu130 [3.41]	Ile214 [5.45]			
Beta-1 adrenergic receptor, engineered, with bound carvedilol, Turkey 4amj									
-5.6	Chl	OH	Glu130 [3.41]	OE2	Glu130 [3.41]	Ile214 [5.45]	Pro219 [5.50]		
	Chl	OH	Ile214 [5.45]	O					
Beta-1 adrenergic receptor, engineered, with bound bucindolol, Turkey 4ami									
-6.1	Chl	OH	Glu130 [3.41]	OE2	Glu130 [3.41]	Ile214 [5.45]			
Beta-1 adrenergic receptor, engineered, with inverse agonist, Turkey 5a8e									
-6.7	Chl	OH	Ser169 [4.53]	OG	Val165 [4.49]	Ile168 [4.52]	Ser169 [4.53]		

Beta-2 adrenergic receptor, active state, complex with antibody, Human 3p0g									
-6.2	Chl	OH	Glu122 [3.41]	OE1	Glu122 [3.41]	Val206 [5.46]			
	Chl	OH	Glu122 [3.41]	OE2					
	Chl	OH	Val206 [5.46]	O					
Beta-2 adrenergic receptor, active state, complex with G-protein, Human 3sn6									
-5.8	Chl	OH	Glu122 [3.41]	OE2	Glu122 [3.41]	Val206 [5.46]			
	Chl	OH	Val206 [5.46]	O					
-5.4	Chl	OH	Glu122 [3.41]	OE2	Glu122 [3.41]				
Beta-2 adrenergic receptor, agonist bound. Human 3pds									
-5.6	Chl	OH	Glu122 [3.41]	OE2	Glu122 [3.41]	Val206 [5.46]			
	Chl	OH	Val206 [5.46]	O					
Beta-2 adrenergic receptor, inactive state, Human 3d4s									
-7.1	Chl	OH	Gly320 [7.47]	O	Val317 [7.43]	Gly320 [7.47]	Phe321 [7.48]		
-6.1	Chl	OH	Ser161 [4.53]	OG	Val157 [4.49]	Ser161 [4.53]			
Beta-2 adrenergic receptor, inactive state, Human 2rh1									
-6.7	Chl	OH	Gly320 [7.47]	O	Val317 [7.43]	Gly320 [7.47]	Phe321 [7.48]		
-5.8	Chl	OH	Gly320 [7.47]	O	Val317 [7.43]	Gly320 [7.47]			

E^1	Donor		Acceptor		Local Residues (within 3 Å of a cholesterol –OH group)				
Beta-2 adrenergic receptor, with allosteric antagonist, Human 5x7d									
-6.0	Chl	OH	Thr164 [4.56]	OG1	Val160 [4.52]	Leu163 [4.55]	Thr164 [4.56]		
C5a anaphylatoxin chemotactic receptor 1, Human 5o9h									
None									
C-C chemokine receptor type 2, Human 5t1a									
-5.9	Chl	OH	Thr296 [7.43]	OG1	Thr296 7.43]	Cys299 [7.47]			
C-C chemokine receptor type 5 with bound Maraviroc Human 4mbs									
None									
C-C chemokine receptor type 9 with vercirnon, Human 5lwe									
None									
C-X-C chemokine receptor type 4, complex with vMIP-II, Human 4rws									
-6.9	Chl	OH	Cys251 [6.47]	O	Cys251 [6.47]	Thr287 [7.37]	Leu290 [7.40]	Ala291 [7.41]	
-6.4	Chl	OH	Ala250 [6.46]	O	Ala250 [6.46]	Cys251 [6.47]			
	Chl	OH	Cys251 [6.47]	O					
-6.0	Chl	OH	Leu208 [5.47]	O	Leu208 [5.47]	Ile209 [5.48]	Gly212 [5.51]		
C-X-C chemokine receptor type 4, inactive, with peptide antagonist CVX15, Human 3oe0									
-7.1	Chl	OH	Cys251 [6.47]	O	Cys251 [6.47]	Thr287 [7.37]	Leu290 [7.40]	Ala291 [7.41]	
-6.9	Chl	OH	Ala250 [6.46]	O	Ala250 [6.46]	Cys251 [6.47]	Pro254 [6.50]		
	Chl	OH	Cys251 [6.47]	O					
-6.3	Chl	OH	Cys251 [6.47]	O	Cys251 [6.47]	Leu290 [7.40]	Ala291 [7.41]		
-6.1	Chl	OH	Gly159 [4.48]	O	Gly159 [4.48]	Val160 [4.49]			
C-X-C chemokine receptor type 4, inactive, with IT1t antagonist, Human 3oe6									
-6.0	Chl	OH	Cys251 [6.47]	O	Cys251 [6.47]	Leu290 [7.40]	Ala291 [7.41]		
-5.7	Chl	OH	Cys251 [6.47]	O	Ala250 [6.46]	Cys251 [6.47]	Pro254 [6.50]		
C-X-C chemokine receptor type 4, with IT1t antagonist, Human 3odu									
-6.8	Chl	OH	Thr168 [4.57]	OG1	Leu165 [4.54]	Thr168 [4.57]	Ile169 [4.59]		
-6.8	Chl	OH	Cys251 [6.47]	O	Ala250 [6.46]	Cys251 [6.47]			
-6.7	Chl	OH	Cys251 [6.47]	O	Cys251 [6.47]	Leu290 [7.40]	Ala291 [7.41]		
-6.3	Chl	OH	Cys251 [6.47]	O	Ala250 [6.46]	Cys251 [6.47]	Pro254 [6.50]		
C-X-C chemokine receptor type 4, with IT1t antagonist, Human 3oe8									
None									
C-X-C chemokine receptor type 4 , with IT1t antagonist, Human 3oe9									
-6.2	Chl	OH	Cys251 [6.47]	O	Cys251 [6.47]	Leu290 [7.40]	Ala291 [7.41]		
-6.2	Chl	OH	Leu86 [2.52]	O	Leu86 [2.52]	Thr90 [2.56]	Ile115 [3.31]		
Cannabinoid receptor 1, complex with antagonist AM6538, Human 5tgz									
-6.2	Chl	OH	Ser284 [5.48]	OG	Val283 [5.47]	Ser284 [5.48]			
-5.7	Chl	OH	Thr391 [7.47]	OG1	Thr391 [7.47]				
Cannabinoid receptor 1, with bound inhibitor taranabant, Human 5u09									
-6.5	Chl	OH	Ser284 [5.48]	OG	Thr283 [5.47]	Ser284 [5.48]			

E^1	Donor		Acceptor		Local Residues (within 3 Å of a cholesterol –OH group)				
Cannabinoid receptor 1, with bound agonist, Human 5xr8									
-7.3	Chl	OH	Ser199 [3.35]	OG	Gly195 [3.31]	Ala198 [3.34]	Ser199 [3.35]		
-6.3	Chl	OH	Thr128 [1.44]	OG1	Gly127 [1.43]	Thr128 [1.44]			
Cannabinoid receptor 1, with bound agonist, Human 5xra									
-7.5	Chl	OH	Thr128 [1.44]	OG1	Leu124 [1.40]	Thr128 [1.44]			
-6.7	Chl	OH	Ser199 [3.35]	OG	Gly195 [3.31]	Ala198 [3.34]	Ser199 [3.35]		
Dopamine D2 receptor complex with risperidone,Human, 6c38									
None									
Dopamine D3 receptor complex with antagonist, Human 3pbl									
None									
Dopamine D4 receptor complex with nemonapride, Human 5wiu									
-7.2	Chl	OH	Thr159 [4.49]	OG1	Phe124 [3.41]	Thr159 [4.49]			
Dopamine D4 receptor Na-bound complex with nemonapride, Human 5wiv									
-6.1	Chl	OH	Thr159 [4.49]	OG1	Phe124. [3.41]	Thr159 4.49]			
-6.1	Chl	OH	Phe202 [5.48]	O	Phe202 [5.48]				
-5.7	Chl	OH	Thr408 [6.49]	OG1	Leu404 [6.45]	Thr408 [6.49]			
Endothelin B receptor without bound endothelin-1, Human 5gli									
None									
Endothelin B receptorwith antagonist, Human 5x93									
None									
Endothelin B receptor, with bound endothelin-1, Human 5glh									
-5.6	Chl	OH	Ser279 [5.45]	OG	Ser279 [5.45]	Phe280 [5.46]			
Free fatty acid receptor 1 GPR40 [PDB residues renumbered], Human 4phu									
-5.5	Chl	OH	Leu235 [6.461]	O	Leu235 [6.461]	Cys2236 [6.47]			
Histamine H1 receptor, complex with doxepin, Human 3rze									
-7.0	Chl	OH	Leu154 [4.52]	O	Leu154 [4.52]	Trp158 [4.57]	Asn198 [5.461]		
Leukotriene BLT1 receptor, Guinea Pig 5x33									
-6.1	Chl	OH	Ser278 [7.46]	OG	Leu275 [7.43]	Ser278 [7.46]			
-6.0	Chl	OH	Ser102 [3.37]	OG	Ile98 [3.33]	Ser102 [3.37]			
Lysophosphatidic acid receptor 1 complex with ONO-9780307, Human 4z34									
-6.2	Chl	OH	Thr173 [4.51]	OG1	Val169 [4.47]	Trp172 [4.50]	Thr173 [4.51]		
Lysophosphatidic acid receptor 1 complex with ONO-9910539, Human 4z35									
-6.2	Chl	OH	Thr173 [4.51]	OG1	Val169 [4.47]	Trp172 [4.50]	Thr173 [4.51]		
Lysophosphatidic acid receptor 1 complex with ONO-3080573, Human 4z36									
-6.2	Chl	OH	Thr173 [4.51]	OG1	Val169 [4.47]	Trp172 [4.50]	Thr173 [4.51]		

E^1	Donor		Acceptor		Local Residues (within 3 Å of a cholesterol –OH group)				
Muscarinic acetylcholine receptor M1 with bound tiotropium, Human 5cxv									
-7.1	Chl	OH	Ser36 [1.43]	OG	Ser36 [1.43]	Gly75 [2.54]	Thr76 [2.55]	Asn80 2.58]	
-5.7	Chl	OH	Ala195 [5.46]	O	Gln110 [3.37]	Ala195 [5.46]	Ala196 [5.461]		
	Chl	OH	Ala196 [5.461]	O					
Muscarinic acetylcholine receptor M2 with bound agonist iperoxo, Human 4mqs									
-7.6	Chl	OH	Ser32 [1.41]	OG	Leu28 [1.37]	Ser32 [1.41]			
-7.1	Chl	OH	Ser32 [1.41]	OG	Leu28 [1.37]	Gly31 [1.40]	Ser32 [1.41]		
Muscarinic acetylcholine receptor M2 with bound antagonist, Human 3uon									
-7.1	Chl	OH	Ser34 [1.43]	OG	Ser34 [1.43]	Asn78 [2.58]			
-6.8	Chl	OH	Ser32 [1.41]	OG	Leu28 [1.37]	Gly31 [1.40]	Ser32 [1.41]		
-6.3	Chl	OH	Ser34 [1.43]	OG	Ser34 [1.43]	Ile38 [1.47]	Gly73 [2.54]	Val74 [2.55]	Asn78 [2.58]
Muscarinic acetylcholine receptor M3, lysozume fusion, with bound tiotropium, Rat 4daj									
-6.9	Chl	OH	Gly117 [2.54]	O	Ala78 [1.43]	Gly117 [2.54]	Asn122 [2.58]		
-5.7	Chl	OH	Ala238 [5.461]	O	Asn152 [3.37]	Val155 [3.40]	Ala238 [5.461]		
Muscarinic acetylcholine receptor M3, lysozyme fusion, with bound tiotropium, Rat 4u15									
-6.8	Trp199 [4.57]	NE1	Chl	O	Asn152 [3.37]	Trp199 [4.57]	Ala238 [5.461]		
-6.1	Chl	OH	Thr504 [6.49]	OG1	Ile500 [6.45]	Thr504 [6.49]			
Muscarinic acetylcholine receptor M4 with bound tiotropium, Human 5dsg									
-7.5	Chl	OH	Ser43 [1.43]	OG	Ser43 [1.43]	Asn87 [2.58]			
-6.8	Chl	OH	Ser41 [1.41]	OG	Thr37 [1.37]	Gly40 [1.40]	Ser41 [1.41]		
-6.0	Chl	OH	Ala203 [5.461]	O	Asn117 [3.37]	Ala203 [5.461]			

Neurotensin receptor type 1,complex with neurotensin, Rat 4grv
None
Neurotensin receptor type 1,agonist bound, Rat 4buo
None
Neurotensin receptor type 1, mutant, Rat 3zev
None
Neurotensin receptor type 1, mutant, Rat 4bv0
None
Neurotensin receptor type 1, engineered, Rat 4xee
None

Neurotensin receptor type 1, engineered, Rat 4xes									
-5.5	Cys152 [3.35]	SG	Chl	O	Leu148 [3.31]	Ala151 [3.34]	Cys152 [3.35]		
Neurotensin receptor type 1, constitutively active mutant, Rat 5t04									
-7.7	Chl	OH	Ser197 [4.53]	OG	Trp194 [4.50]	Ser197 [4.53]	Ala198 [4.54]		

Nociceptin (NOP)receptor with bound C-35, Human 5dhg									
-5.8	Chl	OH	Ser179 [4.54]	OG	Trp175 [4.50]	Ala176 [4.51]	Ser179 [4.54]		
Nociceptin (NOP)receptor, engineered, with bound C-35, Human 5dhh									
-6.1	Chl	OH	Tyr132 [3.34]	OH	Tyr132 [3.34]	Ser179 [4.54]			

E[1]	Donor		Acceptor		Local Residues (within 3 Å of a cholesterol –OH group)				
Nociceptin (NOP)receptor with bound peptide, Human 4ea3									
-5.9	Chl	OH	Ser179 [4.54]	OG	Trp175 [4.50]	Ser179 [4.54]			

Opioid delta receptor comples with naltrindol, Mouse 4ej4									
-6.8	Chl	OH	Ser312 [7.47]	OG	Ala309 [7.43]	Ser312 [7.47]	Leu313 [7.48]		
-6.1	Chl	OH	Tyr130 [3.34]	OH	Tyr130 [3.34]	Ser177 [4.54]			
Opioid delta receptor, complex with naltrindol, Human 4n6h									
None									
Opioid delta receptor, complex with tetrapeptide DIPP-NH2, Human 4rwd									
-6.0	Chl	OH	Tyr130 [3.34]	OH	Tyr130 [3.34]	Ser177 [4.54]			
Opioid delta receptor, complex with tetrapeptide DIPP-NH2, Human 4rwa									
-6.2	Chl	OH	Tyr130 [3.34]	OH	Tyr130 [3.34]	Ser177 [4.54]			

Opioid kappa receptor complex with JDTic, Human 4djh									
-7.3	Chl	OH	Tyr140 [3.34]	OH	Tyr140 [3.34]	Trp183 [4.50]	Ser187 [4.54]		
-6.8	Chl	OH	Ser324 [7.47]	O	Ser324 [7.47]	Leu325 [7.48]			
-6.4	Chl	OH	Ser188 [4.55]	OG	Leu184 [4.51]	Ser188 [4.55]			
-6.3	Ser188 [4.55]	OG	Chl	O	Leu185 [4.52]	Ser188 [4.55]			
-6.2	Chl	OH	Ser324 [7.47]	O	Thr321 [7.43]	Ser324 [7.47]	Leu325 [7.48]		
Opioid kappa receptor, Human 6b73									
-7.8	Chl	OH	Ser188 [4.55]	OG	Leu184 [4.51]	Ser187 [4.54]	Ser188 [4.55]		
-7.7	Chl	OH	Ser187 [4.54]	OG	Leu184 [4.51]	Ser187 [4.54]	Ser188 [4.55]		

Opioid mu receptor, a dimer, complex with morphinan antagonist, Mouse 4dkl									
-6.7	Chl	OH	Tyr149 [3.34]	OH	Tyr149 [3.34]	Ser196 [4.54]			
-5.8	Chl	OH	Ser119 [2.55]	OG	Ala115 [2.51]	Leu116 [2.52]	Ser119 [2.55]		
Opioid mu receptor, bound to agonist BU72, Mouse 5c1m									
-6.6	Chl	OH	Thr153 [3.38]	OG1	Tyr149 [3.34]	Asn150 [3.35]	Thr153 [3.38]		
-5.9	Chl	OH	Thr327 [7.44]	OG1	Ala323 [7.40]	Leu324 [7.41]	Thr327 [7.44]		

Orexin receptor type 1, Human 4zjc
None

Orexin receptor type 2, Human, 4s0v
None
Orexin receptor type 2 plus antagonist, Human, 5wqc
None
Orexin receptor type 2 plus antagonist, Human, 5ws3
None

P2Y purinoceptor 1,complex with BPTU, Human 4xnv									
-6.2	Chl	OH	Ser272 [6.47]	OG	Ser272 [6.47]	Asn316 [7.45]			

E^1	Donor	Acceptor	Local Residues (within 3 Å of a cholesterol –OH group)						
P2Y purinoceptor 1, complex with MRS2500, Human 4xnw									
None									

P2Y purinoceptor 12, complex with antithrombotic drug, Human 4ntj									
-7.2	Chl	OH	Leu75 [2.55]	O	Leu72 [2.52]	Leu75 [2.55]	Thr76 [2.56]		
	Chl	OH	Thr76 [2.56]	OG1					
-6.9	Chl	OH	Ser113 [3.41]	OG	Ser113 [3.41]	Asn201 [5.50]			
-6.3	Chl	OH	Thr76 [2.56]	OG1	Leu72 [2.52]	Thr76 [2.56]	Ile103 [3.31]		
P2Y purinoceptor 12, complex with bound agonist 2MeSADP, Human 4pxz									
-7.1	Chl	OH	Leu72 [2.52]	O	Leu72 [2.52]	Thr76 [2.56]			
	Chl	OH	Thr76 [2.56]	OG1					
-7.1	Chl	OH	Leu72 [2.52]	O	Leu72 [2.52]	Leu75 [2.55]	Thr76 [2.56]		
	Chl	OH	Thr76 [2.56]	OG1					
-5.5	Chl	OH	Leu75 [2.55]	O	Leu75 [2.55]	Thr76 [2.56]			
	Chl	OH	Thr76 [2.56]	OG1					

Sphingosine 1-phosphate (S1P) receptor 1, Human 3v2y									
-7.0	Chl	OH	Ser216 [2.53]	OG	Leu212 [5.49]	Ser216 [2.53]			
-6.6	Chl	OH	Thr211 [5.48]	OG1	Thr208 [5.45]	Thr211 [5.48]	Leu212 [5.49]		
-6.3	Chl	OH	Glu62 [1.49]	OE1	Phe58 [1.45]	Glu62 [1.49]	Gly305 [7.47]		

Thrombin (proteinase-activated) receptor 1, PAR1 with antagonist vorapaxar, Human 3vw7									
-5.5	Chl	OH	Leu150 [2.52]	O	Leu150 [2.52]	Phe151 [2.53]			

Viral GPCR US28, complex with fractalkine, Human herpesvirus 4xt3									
None									
Viral GPCR US28, complex with fractalkine and nanobody, Human herpesvirus 4xt1									
-5.7	Chl	OH	Glu191 [5.41]	OE2	Glu191 [5.41]	Leu194 [5.44]	Gly195 [5.45]		

Rhodopsin and Opsin[2]
Rhodopsin, Bovine 1f88
None
Rhodopsin, Bovine 1l9h
None
Rhodopsin, Bovine 1gzm
None
Rhodopsin, Bovine 1hzx
None
Rhodopsin, Bovine 3c9l
None
Rhodopsin, Bovine 1u19
None
Rhodopsin, with beta-ionone, Bovine 3oax

E^1	Donor	Acceptor	Local Residues (within 3 Å of a cholesterol –OH group)						
None									
Rhodopsin, active (meta-II), without transducin peptide, Bovine 3pxo									
None									
Rhodopsin, active (meta-II), with C-terminal fragment of G-alpha, Bovine 3pqr									
None									
Rhodopsin,consititutionally active (meta-II), with C-terminal fragment of G-alpha, Bovine 4a4m									
None									
Rhodopsin, in agonist-induced active state, Bovine 2x72									
None									
Rhodopsin, complex with arrestin, Human 4zwj									
None									
Rhodopsin, complex with arrestin, Human, 5w0p									
None									

Opsin retinal-free state, Bovine, 5te3									
None									
Opsin, Bovine 5wkt									
None									
Opsin retinal-free state, Bovine 3cap									
-6.0	Thr297 [7.43]	OG1	Chl	O	Thr297 [7.43]	Val300 [7.47]	Tyr301 [7.48]		
-6.0	Chl	OH	Thr297 [7.43]	OG1	Thr297 [7.43]	Tyr301 [7.48]			
	Thr297 [7.43]	OG1	Chl	O					
Opsin retinal-free state with bound G-alpha peptide, Bovine 4j4q									
None									
Opsin retinal-free state with bound G-alpha peptide, Bovine 4x1h									
None									
Opsin retinal-free state with bound ArrFL-1, Bovine 4pxf									
None									
Opsin activated state with bound G-alpha peptide, Bovine 3dqb									
None									

Squid rhodopsin, complex with 11-cis retinal, Japanese flying squid 2z73									
-8.4	Chl	OH	Leu85 [2.55]	O	Gly45 [1.43]	Ser84 [2.54]	Leu85 [2.55]	Phe89 [2.59]	
	Chl	OH	Ser84 [2.54]	O					
	Phe89 [2.59]	N	Chl	O					
-5.8	Chl	OH	Ser275 [6.49]	OG	Leu271 [6.45]	Ser275 [6.49]			
-5.7	Ser273 [6.47]	OG	Chl	O	Gln269 [6.43]	Leu272 [6.46]	Ser273 [6.47]		
Squid rhodopsin, complex with 9-cis isorhodopsin, Japanese flying squid 3ayn									
-7.3	Chl	OH	Leu85 [2.55]	O	Ser84 [2.54]	Leu85 [2.55]	Phe89 [2.59]		

E^1	Donor		Acceptor		Local Residues (within 3 Å of a cholesterol –OH group)				
GPCR Class B[3]									
Corticotropin-releasing factor receptor 1 (CRF1R) with bound antagonist, Human 4k5y									
-6.7	Chl	OH	Thr168 [2.63]	OG1	Leu164 [2.59]	Ala167 [2.62]	Thr168 [2.63]		
-5.7	Chl	OH	Tyr197 [3.38]	OH	Tyr197 [3.38]	Trp236 [4.50]			
Corticotropin-releasing factor receptor 1, (CRF1R) with bound antagonist, Human 4z9g									
-5.9	Chl	OH	Thr168 [2.63]	OG1	Leu164 [2.59]	Thr168 [2.63]			
-5.9	Chl	OH	Tyr197 [3.38]	OH	Tyr197 [3.38]	Trp236 [4.50]			
-5.8	Chl	OH	Thr168 [2.63]	OG1	Leu164 [2.59]	Ala167 [2.62]	Thr168 [2.63]		
Glucagon receptor, Human 4l6r									
-8.9	Chl	OH	Ser189 [2.62]	OG	Leu186 [2.59]	Ser189 [2.62]	Ser190 [2.63]		
	Chl	OH	Ser190 [2.63]	OG					
-8.8	Chl	OH	Leu388 [7.45]	O	Leu388 [7.45]	Phe391 [7.48]	Gln392 [7.49]		
	Chl	OH	Phe391 [7.48]	O					
-7.4	Chl	OH	Leu388 [7.45]	O	His361 [6.52]	Leu388 [7.45]	Gln392 [7.49]		
Glucagon receptor, Human 5xez									
-6.4	Chl	OH	Ser189 [2.62]	OG	Leu186 [2.59]	Ser189 [2.62]	Ser190 [2.63]		
	Ser189 [2.62]	OG	Chl	O					
-5.9	Chl	OH	Gly359 [6.50]	O	Gly359 [6.50]	Val360 [6.51]			
Glucagon receptor, Human 5xf1									
-6.5	Chl	OH	Leu388 [7.45]	O	Leu388 [7.45]	Phe391 [7.48]	Gln392 [7.49]		
Glucagon receptor, with antagonist MK-0893, Human 5ee7									
-5.6	Ser189 [2.62]	OG	Chl	O	Ser189 [2.62]				
Glucagon-like peptide receptor (GLP-1R) complex with NNL0640, Human 5vex									
-6.8	Chl	OH	Leu279 [4.55]	O	Leu279 [4.55]				
-6.1	Chl	OH	Phe390 [7.45]	O	Phe390 [7.45]	Phe393 [7.48]	Gln394 [7.49]		
Glucagon-like peptide receptor (GLP-1R) complex withPF-06372222, Human 5vew									
-6.3	Chl	OH	Leu279 [4.55]	O	Leu279 [4.55]				
GPCR Class C[4]									
Metabotropic glutamate receptor 1, Human 4or2									
-5.7	Chl	OH	Ser715 [4.41]	OG	Ser715 [4.41]	Thr719 [4.45]			
	Chl	OH	Thr719 [4.45]	OG1					
Metabotropic glutamate receptor 5, Human 4oo9									
None									
GPCR Class F[5]									
Smoothened (SMO) receptor with bound antagonist, LY2940680, Human 4jkv									
-5.9	Chl	OH	Ser366 [4.51]	OG	Leu362 [4.47]	Ser366 [4.51]			

E[1]	Donor		Acceptor		Local Residues (within 3 Å of a cholesterol –OH group)				
Smoothened (SMO) receptor with bound SANT-1, Human 4n4w									
-6.0	Chl	OH	Tyr323 [3.34]	OH	Tyr323 [3.34]				
Smoothened (SMO) receptor with bound SAG1.5, Human 4qin									
-6.1	Tyr323 [3.34]	OH	Chl	O	Tyr323 3.34]				
-5.8	Chl	OH	Ser366 [4.51]	OG	Ser366 [4.51]	Leu367 [4.52]			
Smoothened (SMO) receptor with bound ANTA XV, Human 4qim									
None									
Smoothened (SMO) receptor with bound cyclopamine, Human 4o9r									
-5.6	Chl	OH	Ser468 [6.49]	OG	Leu464 [6.45]	Ile465 [6.46]	Ser468 [6.49]		
Smoothened (SMO) receptor in complex with cholesterol, Human 5l7d									
-6.7	Ala324 [3.35]	N	Chl	O	Val319 [3.30]	Ile320 [3.31]	Tyr323 [3.34]	Ala324 [3.35]	
	Chl	OH	Ile320 [3.31]	O					
-6.0	Chl	OH	Leu458 [6.39]	O	Phe457 [6.38]	Leu458 [6.39]	Gly461 [6.42]		
-5.8	Chl	OH	Tyr323 [3.34]	OH	Tyr323 [3.34]	Trp365 [4.50]			
-5.8	Phe462 [6.43]	N	Chl	O	Leu458 [6.39]	Gly461 [6.42]	Phe462 [6.43]		
Smoothened (SMO) receptor with bound vismodegib, Human 5l7i									
-6.4	Ala324 [3.35]	N	Chl	O	Val319 [3.30]	Ile320 [3.31]	Tyr323 [3.34]	Ala324 [3.35]	
	Chl	OH	Ile320 [3.31]	O					

GPCR Adiponectin Receptor[6]

AdipoR1, Human 3wxv									
-6.0	Chl	OH	Thr312 [6]	OG1	Val308 [6]	Thr312 [6]			
AdipoR1,open conformation, Human, 5lxg									
-7.8	Chl	OH	Ser219 [3]	OG	Leu215 [3]	Ile216 [3]	Ser219 [3]		
-6.3	Chl	OH	Thr312 [6]	OG1	Val308 [6]	Ile311 [6]	Thr312 [6]		
AdipoR2, Human, 5lwy									
-6.0	Chl	OH	Ser319 [6]	OG	Met315 [6]	Ala318 [6]	Ser319 [6]		
AdipoR2 complex with fatty acid, Human, 5lx9									
-6.4	Chl	OH	Ser319 [6]	OG	Met315 [6]	Ala318 [6]	Ser319 [6]		
AdipoR2 complex with fatty acid, Human, 5lxa									
-6.6	Chl	OH	Thr323 [6]	OG1	Ser319 [6]	Thr323 [6]			
-6.4	Chl	OH	Ser319 [6]	OG	Met315 [6]	Ser319 [6]			

1. kcals mol^{-1}, with molar concentration units.
2. With residue numbers in the Ballesteros-Weinstein numbering system (1).
3. With residue numbers in the Wootten numbering system (2).
4. With residue numbers in the Pin numbering system (3).
5. With residue numbers in the Wang numbering system (4).
6. With TM helix numbers.

TABLE S2 Channels

[A-J refers to TM subunits as given in the PDB file, followed by the TM helix number; P Pore Helix].

E^1	Donor		Acceptor		Local Residues (within 3 Å of a cholesterol –OH group)			
Ion Channels								
Potassium Channels								
Two-pore domain TWIK-1 human, 3ukm								
-8.3	Chl	OH	Thr225 [A P2]	OG1	Ser224 [A P2]	Thr225 [A P2]		
-8.2	Chl	OH	Thr225 [B P2]	OG1	Thr117 [A P1]	Ser224 [B P2]	Thr225 [B P2]	
-7.6	Chl	OH	Leu115 [A P1]	O	Leu115 [A P1]	Ile142 [A2]		
Two-pore domain TRAAK in non-conductive down state, human, 3um7								
-8.4	Chl	OH	Thr238 [B P2]	OG1	Thr129 [A P1]	Thr237 [B P2]	Thr238 [B P2]	
-8.1	Chl	OH	Ser45 [B1]	OG	Tyr42 [B1]	Ser45 [B1]	Gly46 [B1]	
-7.0	Chl	OH	Thr212 [B3]	OG1	Leu207 [B3]	Leu211 [B3]	Thr212 [B3]	
-7.0	Chl	OH	Leu151 [B2]	O	Leu151 [B2]			
-6.5	Chl	OH	Leu208 [A3]	O	Leu208 [A3]	Pro213 [A3]		
Two-pore domain TRAAK in non-conductive down state in K+, human, 4wff								
-6.6	Chl	OH	Leu236 [A P2]	O	Leu236 [A P2]			
-6.6	Chl	OH	Leu151 [A2]	O	Leu151 [A2]			
-6.4	Chl	OH	Ile127 [B P1]	O	Ile127 [B P1]	Ile154 [B2]	Phe157 [B2]	Gly158 [B2]
-6.4	Chl	OH	Tyr42 [A1]	OH	Tyr42 [A1]	Phe148 [B2]	Tyr149 [B2]	
Two-pore domain TRAAK in non-conductive down state in Tl+, human, 4wfh								
-9.9	Chl	OH	Ile127 [B P1]	O	Ile154 [B2]	Gly158 [B2]		
-8.5	Chl	OH	Thr237 [A P2]	O	Thr237 [A P2]	Thr238 [A P2]		
	Chl	OH	Thr238 [A P2]	OG1				
-8.3	Chl	OH	Leu236 [A P2]	O	Leu236 [A P2]	Thr237 [A P2]		
-8	Chl	OH	Leu151 [A2]	O	Leu151 [A2]			
-6.3	Chl	OH	Tyr42 [A1]	OH	Tyr42 [A1]	Phe148 [B2]	Tyr149 [B2]	
-5.9	Chl	OH	Leu208 [B3]	O	Leu208 [B3]	Pro213 [B3]	Trp264 [B4]	
Two-pore domain TRAAK in conductive up state in K+, human, 4wfe								
6.5	Chl	OH	Tyr42 [B1]	OH	Phe148 [A2]	Tyr149 [A2]	Tyr42 [B1]	
-6.1	Chl	OH	Tyr271 [A4]	OH	Cys206 [A3]	Tyr271 [A4]		
	Tyr271 [A4]	OH	Chl	OH				
Two-pore domain TRAAK in conductive up state in Tl+, human, 4wfg								
-6.6	Tyr42 [A1]	OH	Chl	OH	Tyr42 [A1]	Phe148 [B2]	Tyr149 [B2]	
-6.3	Chl	OH	Tyr42 [A1]	OH	Tyr42 [A1]	Phe148 [B2]	Tyr149 [B2]	
	Tyr42 [A1]	OH	Chl	OH				
Two-pore domain TRAAK, domain-swapped, closed fenestrations, human, 4i9w								
-6.8	Chl	OH	Tyr42 [A1]	OH	Tyr42 [A1]	Phe148 [B2]	Tyr149 [B2]	

E[1]	Donor		Acceptor		Local Residues (within 3 Å of a cholesterol –OH group)			
Two-pore domain TREK-1 up state human, 4twk								
-7.5	Chl	OH	Tyr284 [A4]	OH	Ile215 [A3]	Tyr284 [A4]		
-6.1	Chl	OH	Tyr57 [B1]	OH	Ile161 [A2]	Tyr162 [A2]	Leu165 [A2]	Tyr57 [B1]
Two-pore domain TREK-1 up state mouse, 5vk5								
-6.2	Chl	OH	Tyr57 [A1]	OH	Tyr57 [A1]	Ile161 [B2]	Tyr162 [B2]	
-5.9	Chl	OH	Leu221 [A3]	O	Leu221 [A3]	Pro226 [A1]	Trp277 [A4]	
Two-pore domain TREK-1 up state mouse, 5vkn								
-5.6	Chl	OH	Tyr284 [A4]	OH	Cys219 [A3]	Tyr284 [A4]		
-5.5	Chl	OH	Leu221 [A3]	O	Leu221 [A3]	Phe222 [A3]		
Two-pore domain TREK-1 complex with ML402, mouse, 5vkp								
-5.6	Chl	OH	Leu221 [A3]	O	Leu221 [A3]	Trp277 [A4]		
Two-pore domain TREK-2 up state human, 4bw5								
-6.6	Chl	OH	Tyr87 [A1]	OH	Tyr87 [A1]	Leu191 [B2]	Tyr192 [B2]	Tyr87 [B1]
Two-pore domain TREK-2 down state human (res. 3.8 A), 4xdj								
-8.1	Chl	OH	Thr281 [A P2]	OG1	Thr280 [A P2]	Thr281 [A P2]		
-7.8	Chl	OH	Ile194 [A2]	O	Ile194 [A2]			
-7.6	Chl	OH	Leu279 [B P2]	O	Leu279 [B P2]			
Two-pore domain TREK-2 down state, Br-fluoxetine bound, human, 4xdl								
-8.2	Chl	OH	Ile194 [C2]	O	Ile194 [C2]			
-8.2	Chl	OH	Thr281 [D P2]	OG1	Thr280 [D P2]	Thr281 [D P2]		
Two-pore domain TREK-2 down state, norfluoxetine bound (res 3.6 Å), human, 4xdk								
-8.4	Chl	OH	Ile170 [A P1]	O	Ile197 [A2]	Gly201 [A2]		
-8.2	Chl	OH	Leu279 [B P2]	O	Leu279 [B P2]	Thr280 [B P2]	Thr281 [B P2]	

Voltage-gated channel Kv1.2, rat, 3lut								
None								
Voltage-gated channel Kv1.2, rat, 2a79								
-8.0	Chl	OH	Thr401 [A6]	OG1	Phe334 [A5]	Thr401 [A6]		
-7.9	Chl	OH	Thr401 [A6]	OG1	Ala397 [A5]	Thr401 [A6]		
Voltage-gated channel Kv1.2/Kv2.1 paddle chimera [PDB numbering changed to match 2a79], rat, 2r9r								
-6.3	Chl	OH	Thr401 [A6]	OG1	Phe334 [A5]	Gly338 [A5]	Thr401 [A6]	
Voltage-gated channel Kv1.2/Kv2.1 paddle chimera [PDB numbering changed to match 2a79] rat, 3lnm								
-7.8	Chl	OH	Thr401 [A6]	OG1	Phe334 [A5]	Gly338 [A5]	Met372 [A P]	Thr401 [A6]
Voltage-gated channel Kv1.2/Kv2.1 paddle chimera, inactivated V410W mutant, rat, 5wie								
None								

Inward-rectifier Kir 2.2 chicken, 3jyc								
-6.7	Trp94 [A1]	NE1	Chl	O	Trp94 [A1]	Gln141 [A P]		
Inward-rectifier Kir 2.2 mutant apo form, 3spj								
-9.1	Chl	OH	Gln141 [A P]	O	Gln141 [A P]	Ser166 [A2]	Gly169 [A2]	Cys170 [A2]
-7.7	Trp94 [A1]	NE1	Chl	O	Phe90 [A1]	Trp94 [A1]	Gln141 [A P]	
Inward-rectifier Kir 2.2 in complex with PIP2 chicken, 3spi								
-7.0	Chl	OH	Gln141 [A P]	O	Gln141 [A P]	Ser166 [A2]	Gly169 [A2]	Cys170 [A2]

E^1	Donor	Acceptor	Local Residues (within 3 Å of a cholesterol –OH group)
Inward-rectifier Kir 2.2 mutant in complex with PIP2 chicken, 3spg			
None			
Inward-rectifier Kir 2.2 mutant in complex with PIP2 chicken, 3sph			
None			
Inward-rectifier Kir 2.2 in complex with PPA chicken, 3spc			
None			
Inward-rectifier Kir 2.2 K62W mutant chicken, 5kuk			
None			

G-protein gated channel, GIRK2 (Kir 3.2) wild type. mouse, 3syo								
-7.0	Chl	OH	Ser181 [A2]	OG	Ser177 [A2]	Gly180 [A2]	Ser181 [A2]	
G-protein gated channel, GIRK2 (Kir 3.2) D228N mutant. mouse, 3syc								
-6.1	Chl	OH	Tyr102 [A1]	OH	Tyr102 [A1]			
	Tyr102 [A1]	OH	Chl	OH				
-6.0	Chl	OH	Glu152 [B P]	OE2	Tyr102 [B1]	Glu152 [B P]		
	Tyr102 [B1]	OH	Chl	OH				
G-protein gated channel, GIRK2 (Kir 3.2) wild type plus PIP2, mouse, 3sya								
-7.2	Chl	OH	Ser181 [A2]	OG	Ser177 [A2]	Ser181 [A2]	Tyr102 [D1]	
G-protein gated channel, GIRK2 (Kir 3.2) R201A mutant plus PIP2, mouse, 3syq								
-9.1	Chl	OH	Ser181 [C2]	OG	Ser177 [C2]	Ser181 [C2]		
-9.1	Chl	OH	Glu152 [B P]	O	Glu152 [B P]	Gly180 [B2]		
	Chl	OH	Gly180 [B2]	O				
-7.9	Chl	OH	Ser177 [B2]	O	Ser177 [B2]	Gly180 [B2]	Ser181 [B2]	
	Chl	OH	Ser181 [B2]	OG				
-7.5	Chl	OH	Tyr102 [D1]	OH	Tyr102 [D1]	Asn184 [D2]		
	Tyr102 [D1]	OH	Chl	OH				
G-protein gated channel, GIRK2 (Kir 3.2) plus G-protein subunits. mouse, 4kfm								
-9.6	Chl	OH	Ser181 [F2]	OG	Ser177 [F2]	Ser181 [F2]		
-8.9	Chl	OH	Glu152 [J P]	O	Glu152 [J P]	Gly180 [J2]		
	Chl	OH	Glu152 [J P]	OE2				
-8.5	Chl	OH	Ser181 [A2]	OG	Ser181 [A2]	Asn184 [J2]		

Calcium-activated channel Slo1 (BK) sea slug, 5tj6								
-7.5	Chl	OH	Ser29 [A1]	OG	Thr26 [A1]	Ser29 [A1]	Gly30 [A1]	

Lysosomal K+-selective channel TMEM175 homolog, marine worm, 5vre
None

Calcium-ion selective Channels

Orai calcium release-activated CRAC channel, Drosophila, 4hkr								
-6.8	Chl	OH	Thr283 [A4]	O	Thr283 [A4]	Leu286 [A4]	Ile287 [A4]	
Orai calcium release-activated CRAC channel mutant, Drosophila, 4hks								
-6.6	Chl	OH	Thr283 [A4]	O	Thr283 [A4]	Leu286 [A4]	Ile287 [A4]	

E^1	Donor		Acceptor		Local Residues (within 3 Å of a cholesterol –OH group)			
Transient Receptor Potential (TRP) Channels								
TRPM4 cation channel, apo state, human, 6bcj								
None								
TRPM4 cation channel, apo state, human, 6bcl								
None								
TRPM4 cation channel, ATP bound, human, 6bco								
None								
TRPM4 cation channel, ATP bound, human, 6bcq								
None								
TRPM4 cation channel, Ca-free, human, 6bqr								
None								
TRPM4 cation channel, Ca-bound, human, 6bqv								
None								
TRPML1, human, 5wj9								
-7.8	Chl	OH	Tyr439 [A5]	OH	Tyr439 [A5]	Ser500 [A6]		
-6.9	Chl	OH	Ser503 [A6]	OG	Tyr499 [A6]	Ser503 [A6]		
TRPML3, marmoset, 5w3s								
-7.1	Chl	OH	Tyr491 [A6]	OH	Tyr491 [A6]	Ile455 [D P]		
	Tyr491 [A6]	OH	Chl	OH				
TRPV1 rat, 3j5p								
-7.7	Chl	OH	Thr550 [A4]	OG1	Met547 [A4]	Thr550 [A4]	Asn551 [A4]	
-7.5	Chl	OH	Ser483 [A2]	OG	Ser483 [A2]	Gly484 [A2]		
	Ser483 [A2]	OG	Chl	OH				
TRPV1 rat, 5irz								
-8.2	Chl	OH	Ser483 [A2]	OG	Ser483 [A2]	Gly484 [A2]		
	Ser483 [A2]	OG	Chl	OH				
-8.0	Chl	OH	Thr550 [A4]	OG1	Ala546 [A4]	Met547 [A4]	Thr550 [A4]	
TRPV1 complex with DkTx and RTX, rat, 5irx								
-8.6	Chl	OH	Thr550 [A4]	OG1	Ala546 [A4]	Met547 [A4]	Thr550 [A4]	
-6.9	Chl	OH	Ser483 [A2]	OG	Ser483 [A2]	Gly484 [A2]		
	Ser483 [A2]	OG	Chl	OH	Ser483 [A2]	Gly484 [A2]		
TRPV1 complex with capsaicin, rat, 5is0								
-8.7	Chl	OH	Thr550 [A4]	OG1	Ala546 [A4]	Met547 [A4]	Thr550 [A4]	
-6.6	Chl	OH	Ser483 [A2]	OG	Ile479 [A2]	Val482 [A2]	Ser483 [A2]	
TRPV6 rat, 5iwk								
None								
TRPV6 rat, 5wo6								
-5.8	Chl	OH	Thr430 [A3]	OG1	Val426 [A3]	Ile427 [A3]	Thr430 [A3]	
TRPV6 rat, 5wo7								
-6.3	Chl	OH	Val498 [A5]	O	Val498 [A5]	Val499 [A5]	Gly502 [A5]	
TRPV6-Del1, rat, 5wo8								
-6.1	Chl	OH	Thr430 [A3]	OG1	Val426 [A3]	Ile427 [A3]	Thr430 [A3]	

E[1]	Donor		Acceptor		Local Residues (within 3 Å of a cholesterol –OH group)			
TRPV6, plus Ca2+, rat, 5wo9								
-7.1	Chl	OH	Cys462 [A4]	O	Trp461 [A4]	Cys462 [A4]	Val464 [A4]	Met465 [A4]
	Met465 [A4]	N	Chl	OH				

PKD2 polycystic kidney disease channel, human, 5t4d								
-6.7	Chl	OH	Thr663 [A6]	OG1	Tyr611 [A5]	Thr663 [A6]		
	Tyr611 [A5]	OH	Chl	OH				

Glutamate Receptors

GluA2 glutamate receptor (AMPA) apo form A, rat, 4u2p								
-9.1	Tyr533 [A1]	OH	Chl	OH	Tyr533 [A1]	Arg599 [D2]		
-8.2	Chl	OH	Thr609 [A2]	OG1	Trp605 [A2]	Thr609 [A2]		
-7.3	Chl	OH	Thr609 [A2]	OG1	Trp605 [A2]	Thr609 [A2]		
	Trp605 [A2]	NE1	Chl	OH				
GluA2 glutamate receptor (AMPA) with kainate crystal form A, rat, 4u1w								
-7.8	Chl	OH	Thr609 [A2]	OG1	Trp605 [A2]	Thr609 [A2]		
-7.5	Trp605 [A2]	NE1	Chl	OH	Trp605 [A2]	Thr609 [A2]		
GluA2 glutamate receptor (AMPA) with kainate crystal form B, rat, 4u1x								
-7.6	Chl	OH	Thr609 [A2]	OG1	Thr609 [A2]			
-6.8	Chl	OH	Thr609 [A2]	OG1	Thr609 [A2]	Trp606 [D2]		
GluA2 glutamate receptor (AMPA) mutant with toxin etc, rat, 4u5b								
-9.2	Tyr533 [C1]	OH	Chl	OH	Arg599 [B2]	Tyr533 [C1]		
-8.3	Chl	OH	Thr609 [A2]	OG1	Trp605 [A2]	Thr609 [A2]		
	Trp605 [A2]	NE1	Chl	OH				
-7.7	Trp605 [A2]	NE1	Chl	OH	Trp605 [A2]			

P2X channels

ATP-gated P2X3 channel closed apo state, human, 5svj								
-6.9	Chl	OH	Thr336 [A2]	OG1	Gly333 [A2]	Thr336 [A2]		
ATP-gated P2X3 channel ATP bound open state, human, 5svk								
-7.7	Chl	OH	Ser331[A2]	OG	Thr330 [A2]	Ser331 [A2]		
	Chl	OH	Thr330 [A2]	OG1				
	Chl	OH	Thr330 [A2]	O				
-6.2	Chl	OH	Ser36 [A1]	OG1	Leu33 [A1]	Ser36 [A1]	Tyr37 [A1]	
ATP-gated P2X3 channel ATP-bound, desensitized state, human, 5svl								
-8.9	Chl	OH	Thr330 [A2]	OG1	Thr330 [A2]	Ser331 [A2]		
-8.9	Chl	OH	Ser331 [A2]	OG	Thr330 [A2]	Ser331 [A2]		
ATP-gated P2X3 channel agonist bound desensitized state, human, 5svm								
-11.4	Chl	OH	Ser331 [A2]	OG	Ala327 [A2]	Thr330 [A2]	Ser331 [A2]	
	Chl	OH	Thr330 [A2]	OG1				
ATP-gated P2X3 channel agonist bound desensitized state, human, 5svp								
-11.4	Chl	OH	Ser331 [A2]	OG	Ala327 [A2]	Thr330 [A2]	Ser331 [A2]	
	Chl	OH	Thr330 [A2]	OG1				
ATP-gated P2X3 channel competitive antagonist bound closed state, human, 5svq								
None								

E[1]	Donor		Acceptor		Local Residues (within 3 Å of a cholesterol –OH group)			
ATP-gated P2X3 channel competitive antagonist bound closed state, human, 5svr								
-6.6	Chl	OH	Ser36 [A1]	OG	Ser36 [A1]			
-6.3	Chl	OH	Thr336 [A2]	OG1	Val332 [A2]	Gly333 [A2]	Thr336 [A2]	
ATP-gated P2X4 channel apo state, zebra fish, 3h9v								
None								
ATP-gated P2X4 channel apo closed state, zebra fish, 3i5d								
None								
ATP-gated P2X4 channel plus CTP open state, zebra fish, 5wzy								
-6.9	Chl	OH	Ala344 [A2]	O	Ala344 [A2]	Ala347 [A2]	Leu348 [A2]	
ATP-gated P2X4 channel ATP bound open state, zebra fish, 4dw1								
-7.3	Chl	OH	Gly343 [A2]	O	Gly343 [A2]	Ala344 [A2]		
ATP-gated P2X4 channel ATP-free closed state, zebra fish, 4dw0								
None								
ATP-gated P2X4 channel ATP bound open state, Gulf Coast tick, 5f1c								
None								
ATP-gated P2X7 channel plus competitive antagonist, chicken, 5xw6								
-8.4	Chl	OH	Ser326 [B2]	OG	Thr322 [B2]	Ser326 [B2]		
-6.6	Chl	OH	Tyr330 [C2]	OH	Tyr330 [C2]			
-6.5	Chl	OH	Thr327 [C2]	OG1	Thr327 [C2]	Ile328 [C2]		
	Thr327 [C2]	OG1	Chl	OH				
Acid-sensing ion-channel (ASIC), chicken, 4nyk								
None								
Chloride channels								
Bestrophin-1 (BEST1) Ca-activated Cl channel, jungle fowl, 4rdq								
-9.5	Chl	OH	Ala73 [A2]	O	Asn70 [A2]	Ser71 [A2]	Ala73 [A2]	Glu74 [A2]
Bestrophin-1 (BEST1) Ca-activated Cl channel mutant, jungle fowl, 5t5n								
-8.9	Chl	OH	Ala73 [A2]	O	Asn70 [A2]	Ala73 [A2]	Arg255 [A3]	
Neurotransmitter-gated ion channels of the Cys-loop receptor family								
Glycine receptor complex with strychnine, human, 5cfb								
-7.2	Chl	OH	Ser296 [A3]	OG	Leu292 [A3]	Ser296 [A3]		
Glycine receptor complex with AM-3607, human, 5tio								
-7.5	Chl	OH	Ser296 [A3]	OG	Leu292 [A3]	Ser296 [A3]		
Glycine receptor, mutant, complex with AM-3607, human, 5tin								
-8.3	Chl	OH	Ser296 [A3]	OG	Leu292 [A3]	Phe293 [A3]	Ser296 [A3]	
Glycine receptor, complex with Gly and ivermectin, human, 5vdh								
-8.0	Chl	OH	Ser296 [A3]	OG	Leu292 [A3]	Phe293 [A3]	Ser296 [A3]	
GABA-A receptor (β3 homopentamer), human, 4cof								
-7.5	Chl	OH	Ser436 [A4]	OG	Pro432 [A4]	Phe435 [A4]	Ser436 [A4]	
GABA-A receptor (α5 TMD - β3 ECD chimera) with pregnanolone, human, 5o8f								
-8.1	Chl	OH	Ser302 [A3]	OG	Ala298 [A3]	Ser302 [A3]		
	Ser302 [A3]	OG	Chl	OH				
-7.5	Chl	OH	Thr408 [A4]	OG1	Leu405 [A4]	Thr408 [A4]	Phe409 [A4]	

E^1	Donor		Acceptor		Local Residues (within 3 Å of a cholesterol –OH group)			
Serotonin 5-HT3 receptor, mouse, 4pir								
-7.6	Chl	OH	Thr445 [A4]	OG1	Ala441 [A4]	Tyr442 [A4]	Thr445 [A4]	

Porins etc.

AQPO aquaporin lens, cow, 1ymg								
None								
AQPO aquaporin lens, sheep, 1sor								
None								
AQPO aquaporinn lens, sheep, 2b6o								
None								
AQPO aquaporin lens, sheep, 2b6p								
None								
AQPO aquaporin lens, sheep, 3m9i								
None								
AQP1 aquaporin red blood cell, human, 4csk								
None								
AQP1 aquaporin red blood cell, cow, 1j4n								
None								
AQP2 aquaporin, kidney, human, 4nef								
None								
AQP4 aquaporin glial cell, rat, 2d57								
-5.8	Chl	OH	Thr120 [A3]	OG1	Thr120 [A3]			
AQP4 aquaporin glial cell, mutant, rat, 2zz9								
-5.7	Chl	OH	Thr120 [A3]	OG1	Thr120 [A3]			
AQP4 aquaporin, human, 3gd8								
None								
AQP5 aquaporin, human, 3d9s								
None								
SoPIP2 plant aquaporin, spinach, mutant, 3cll								
None								
SoPIP2 plant aquaporin, spinach, mutant, 3cn5								
None								
SoPIP2 plant aquaporin, spinach, mutant, 3cn6								
None								
TIP2, ammonia-permeable aquaporin, Arabidopsis, 5i32								
None								
Urea Transporters								
UT-B, cow, 4ezc								
-7.6	Chl	OH	Ala147 [A3]	O	Ala147 [A3]	Thr151 [A3]		
	Chl	OH	Thr151 [A3]	OG1				
	Thr151 [A3]	OG1	Chl	OH				
UT-B bound to selenourea, cow, 4ezd								
-7.0	Chl	OH	Thr151 [A3]	OG1	Ala147 [A3]	Thr151 [A3]		

E[1]	Donor	Acceptor	Local Residues (within 3 Å of a cholesterol –OH group)
Rh ammonia channel			
Rh C glycoprotein ammonia transporter, human, 3hd6			
None			

1. kcals mol^{-1}, with molar concentration units.

TABLE S3 Transporters [With subunits as given in the PDB file, and TM helix number]

E[1]	Donor		Acceptor		Local Residues (within 3 Å of a cholesterol –OH group)			
ATPases								
Calcium ATPase [B sarcolipin; C phospholamban]								
E1 with bound Ca and AMPPCP, rabbit 1vfp								
-6.1	Chl	OH	Ser942 [9]	OG	Cys938 [9]	Met941 [9]	Ser942 [9]	
-5.9	Chl	OH	Leu797 [6]	O	Leu797 [6]	Leu802 [6]	Ser940 [9]	
E1 with bound Ca, rabbit 1su4								
-6.4	Chl	OH	Ser942 [9]	OG	Cys938 [9]	Ser942 [9]		
-6.2	Chl	OH	Met909 [8]	O	Thr906 [8]	Met909 [8]	Cys910 [8]	
-5.8	Gly979 [10]	N	Chl	O	Leu975 [10]	Gly979 [10]		
E1 with bound Ca, rabbit, 2c9m								
-7.0	Chl	OH	Thr906 [8]	OG1	Thr906 [8]	Cys910 [8]		
	Thr906 [8]	OG1	Chl	OH				
-6.1	Chl	OH	Gly842 [7]	O	Gly842 [7]			
Structure in ultrathin crystals, rabbit, 3j7t								
-6.4	Chl	OH	Ser942 [9]	OG	Cys938 [9]	Ser942 [9]		
E1 Mg bound state with TNPAMP, rabbit, 3w5b								
-6.3	Chl	OH	Ser942 [9]	OG	Cys938 [9]	Ser942 [9]		
Ca bound phosphorylated form with AMPPN, rabbit 3ba6								
-7.0	Chl	OH	Leu797 [6]	O	Leu797 [6]	Val798 [6]	Ser940 [9]	
-6.4	Chl	OH	Ala839 [7]	O	Met838 [7]	Ala839 [7]	Gly842 [7]	Tyr843 [7]
-6.4	Chl	OH	Ser942 [9]	OG	Cys938 [9]	Ser942 [9]		
-6.3	Chl	OH	Met909 [8]	O	Thr906 [8]	Met909 [8]	Cys910 [8]	
	Chl	OH	Thr906 [8]	O				
E1 with bound Ca and AMPPCP, rabbit 1t5s								
-6.9	Chl	OH	Met909 [8]	O	Thr906 [8]	Met909 [8]	Cys910 [8]	
	Chl	OH	Thr906 [8]	O				
E1 state with bound Ca and AMPPCP, rabbit, 4xou								
-7.3	Chl	OH	Leu797 [6]	O	Leu797 [6]	Val798 [6]	Ser940 [9]	
-6.9	Chl	OH	Ser940 [9]	OG	Leu797 [6]	Val798 [6]	Ser940 [9]	
-6.4	Chl	OH	Ala839 [7]	O	Met838 [7]	Ala839 [7]	Gly842 [7]	Tyr843 [7]
	Tyr843 [7]	N	Chl	OH				
E1 Ca bound state mutant with AMPPCP, rabbit, 4nab								
None								
E2 State with phosphate, rabbit, 3w5d								
-6.7	Chl	OH	Ser942 [9]	OG	Cys938 [9]	Met941 [9]	Ser942 [9]	
E2 state, and thapsigargin, rabbit 1iwo								
-6.7	Chl	OH	Tyr295 [4]	O	Tyr295 [4]			
E2 thapsigargin compex, rabbit, 5xab								
-6.3	Chl	OH	Ser942 [9]	OG	Cys938 [9]	Ser942 [9]		
-6.2	Chl	OH	Tyr295 [4]	O	Tyr295 [4]			
E2 state, Ca free with thapsigargin, rabbit, 2c8l								
-6.6	Cys910 [8]	SG	Chl	OH	Thr906 [8]	Cys910 [8]		
-6.2	Chl	OH	Tyr295 [4]	O	Tyr295 [4]			

E^1	Donor		Acceptor		Local Residues (within 3 Å of a cholesterol –OH group)			
With bound thapsigargin, rabbit, 2ear								
-7.2	Chl	OH	Cys268 [3]	O	Cys268 [3]	Trp272 [3]		
	Trp272 [3]	N	Chl	OH				
-6.3	Trp794 [6]	N	Chl	OH	Val790 [6]	Trp794 [6]		
E2 state and magnesium fluoride rabbit 1wpg								
5.7	Trp794 [6]	N	Chl	O	Val790 [6]	Leu793 [6]	Trp794 [6]	
E2 state and thapsigargin and aluminium fluoride rabbit 1xp5								
-6.0	Chl	OH	Tyr295 [4]	O	Tyr295 [4]			
E2 state, Ca free with thapsigargin and AMPPCP, rabbit, 2c8k								
-6.3	Cys910 [8]	SG	Chl	OH	Thr906 [8]	Cys910 [8]		
E2 state and AMPPN and aluminium fluoride rabbit 3b9r								
-6.5	Chl	OH	Pro91 [2]	O	Ala69 [1]	Pro91 [2]	Leu95 [2]	
E2-Pi state and beryllium fluoride rabbit 3b9b								
None								
With bound BHQ and thapsigargin, rabbit 2agv								
None								
With bound thapsigargin derivative, rabbit 2by4								
-7.4	Chl	OH	Val790 [6]	O	Val790 [6]	Leu793 [6]	Trp794 [6]	
-6.4	Chl	OH	Leu975 [10]	O	Leu975 [10]	Pro976 [10]	Gly979 [10]	
E2 Ca free state with dibutanoyl thapsigargin, 2yfy								
-6.7	Chl	OH	Ser942 [9]	OG	Cys938 [9]	Met941 [9]	Ser942 [9]	
With bound thapsigargin and AMPPCP, rabbit 2c88								
-6.6	Chl	OH	Tyr295 [4]	O	Tyr295 [4]	Ala299 [4]		
-6.3	Chl	OH	Gly842 [7]	O	Ala839 [7]	Gly842 [7]	Tyr843 [7]	
-6.2	Cys910 [8]	SG	Chl	O	Thr906 [8]	Met909 [8]	Cys910 [8]	
With bound CPA and thapsigargin, rabbit, 2eat								
-6.2	Chl	OH	Pro91 [2]	O	Ala69 [1]	Pro91 [2]		
-6	Chl	OH	Leu266 [3]	O	Leu266 [3]	Ile267 [3]		
-5.7	Chl	OH	Leu793 [6]	O	Leu793 [6]	Trp794 [6]		
With bound CPA and curcumin, rabbit, 2eau								
None								
With bound cyclopiazonic acid and aluminium fluoride, rabbit 2o9j								
-6.8	Chl	OH	Val790 [6]	O	Val790 [6]	Leu793 [6]	Trp794 [6]	
-5.9	Cys910 [8]	SG	Chl	O	Thr906 [8]	Cys910 [8]		
-5.6	Chl	OH	Ala270 [3]	O	Ala270 [3]	Leu273 [3]		
	Chl	OH	Leu273 [3]	O				
With bound cyclopiazonic acid and ADP, rabbit, 2oao								
-7.2	Chl	OH	Val790 [6]	O	Val790 [6]	Trp794 [6]		
-5.9	Chl	OH	Gly842 [7]	O	Ala839 [7]	Gly842 [7]	Tyr843 [7]	
E2-vandate complex with thapsigargin and TNP-AMPPCP, rabbit, 5a3q								
-6.1	Chl	OH	Cys268 [3]	O	Cys268 [3]	Trp272 [3]		
	Trp272 [3]	N	Chl	OH				

E[1]	Donor		Acceptor		Local Residues (within 3 Å of a cholesterol –OH group)			
E2-vanadate complex with thapsigargin and TNP-ATPP, rabbit, 5a3s								
-5.9	Chl	OH	Tyr295 [4]	O	Tyr295 [4]			
-5.7	Cys70 [1]	N	Chl	OH	Leu66 [1]	Cys70 [1]		
-5.7	Chl	OH	Cys268 [3]	O	Cys268 [3]	Trp272 [3]		
E2-BeF3 complex with TNP-AMPPCP, rabbit, 5a3r								
-6.6	Chl	OH	Ile264 [3]	O	Ile264 [3]	Ser265 [3]		
	Chl	OH	Ser265 [3]	OG				
-6.0	Chl	OH	Ala306 [4]	O	Ala306 [4]			
-5.9	Chl	OH	Ala69 [1]	O	Ala69 [1]	Pro91 [2]		
E1-Ca bound with lipid, rabbit, 5xa7								
-6.4	Chl	OH	Ser942 [9]	OG	Cys938 [9]	Ser942 [9]		
-6.1	Chl	OH	Met909 [8]	O	Met909 [8]	Leu913 [8]		
-6.0	Gly979 [10]	N	Chl	OH	Leu975 [10]	Pro976 [10]	Gly979 [10]	
E1-AlF4 complex with Ca and ADP, rabbit, 5xa8								
-6.4	Chl	OH	Leu797 [6]	O	Leu797 [6]	Val798 [6]	Ser940 [9]	
	Chl	OH	Ser940 [9]	OG				
E2-AlF4 complex with thapsigargin, , rabbit, 5xa9								
-6.9	Chl	OH	Val790 [6]	O	Val790 [6]	Trp794 [6]		
	Trp794 [6]	N	Chl	OH				
E2-AlF4 complex with thapsigargin, different crystal form, rabbit, 5xaa								
-6.7	Chl	OH	Cys268 [3]	O	Cys268 [3]	Tyr295 [4]		
	Chl	OH	Tyr295 [4]	OH				
-6.4	Chl	OH	Val790 [6]	O	Val790 [6]	Leu793 [6]	Trp794 [6]	
-6.1	Chl	OH	Pro91 [2]	O	Ala69 [1]	Pro91 [2]	Ile94 [2]	
-5.9	Chl	OH	Pro976 [10]	O	Leu975 [10]	Pro976 [10]	Ile978 [10]	Gly979 [10]
	Gly979 [10]	N	Chl	OH				
With bound tetrahydrocarbazole and TNP-ATP, rabbit, 5ncq								
None								
E1 with bound Ca and sarcolipin, rabbit 4h1w								
-6.9	Chl	OH	Thr18 [B]	OG1	Val14 [B]	Thr18 [B]		
-6.2	Chl	OH	Thr18 [B]	OG1	Leu96 [2]	Ala100 [2]	Thr18 [B]	
-6.2	Chl	OH	Cys268 [3]	O	Cys268 [3]	Val269 [3]		
With sarcolipin and magnesium in E1 state, rabbit 3w5a								
-6.1	Chl	OH	Cys268 [3]	O	Cys268 [3]	Val269 [3]		
-6.0	Gly979 [10]	N	Chl	O	Leu975 [10]	Gly979 [10]		
With two bound phospholamban, rabbit 4kyt								
7.0	Chl	OH	Ile33 [C]	O	Ile33 [C]	Asn34 [C]		
-6.3	Chl	OH	Ser974 [10]	OG	Thr906 [8]	Cys910 [8]	Ser974 [10]	
	Cys910 [8]	SG	Chl	O				
SERCA pig heart, 5mpm								
None								

E^1	Donor		Acceptor		Local Residues (within 3 Å of a cholesterol –OH group)			
Na,K- ATPase [A, alpha subunit; B, β1 subunit; G, γ subunit]								
Pig kidney, 3b8e								
-7.0	Chl	OH	Leu46 [B]	O	Tyr43 [B]	Leu46 [B]	Ala47 [B]	
-6.6	Chl	OH	Ser298 [A 3]	OG	Phe294 [A 3]	Ser298 [A 3]		
-6.5	Chl	OH	Gly806 [A 6]	O	Gly806 [A 6]	Thr807 [A 6]	Val810 [A 6]	
-6.4	Chl	OH	Leu36 [G]	O	Leu36 [G]			
-6.4	Chl	OH	Glu953 [A 9]	OE2	Glu953 [A 9]			
-6.3	Chl	OH	Ala101 [A 1]	O	Trp98 [A 1]	Ala101 [A 1]	Ile102 [A 1]	
Pig kidney with bound Na, pre-E1P state without oligomycin, 3wgu								
-8.0	Chl	OH	Ser988 [A 10]	OG	Ala925 [A 8]	Ser988 [A 10]	Leu989 [A 10]	
-7.2	Chl	OH	Glu953 [A 9]	OE1	Glu953 [A 9]	Leu957 [A 9]		
-7.1	Chl	OH	Gly806 [A 6]	O	Leu805 [A 6]	Gly806 [A 6]	Met809 [A 6]	Val810 [A 6]
	Chl	OH	Leu805 [A 6]	O				
Pig kidney with bound Na, pre-E1P state with oligomycin, 3wgv								
-6.8	Chl	OH	Gly806 [A 6]	O	Gly806 [A 6]	Glu954 [A 9]		
-6.7	Chl	OH	Gly806 [A 6]	O	Leu805 [A 6]	Gly806 [A 6]	Val810 [A 6]	
	Chl	OH	Leu805 [A 6]	O				
-6.5	Chl	OH	Glu953 [A 9]	OE1	Glu953 [A 9]			
Pig kidney with bound Rb (K analogue), 3kdp								
-7.1	Chl	OH	Leu36 [G]	O	Phe33 [G]	Leu36 [G]		
	Chl	OH	Phe33 [G]	O				
-6.9	Thr955 [A 9]	OG1	Chl	O	Trp924 [A 8]	Thr955 [A 9]		
-6.8	Thr955 [A 9]	OG1	Chl	O	Leu951 [A 9]	Phe952 [A 9]	Thr955 [A 9]	
-6.6	Chl	OH	Gly806 [A 6]	O	Leu805 [A 6]	Gly806 [A 6]		
	Chl	OH	Leu805 [A 6]	O				
-6.4	Ala925 [A 8]	N	Chl	O	Val921 [A 8]	Trp924 [A 8]	Ala925 [A 8]	Ser988 [A 10]
	Chl	OH	Ser988 [A 10]	OG				
-6.3	Chl	OH	Glu953 [A 9]	OE2	Gly806 [A 6]	Glu953 [A 9]		
	Chl	OH	Gly806 [A 6]	O				
Pig kidney phosphorylated form with bufalin, 4res								
-7.9	Thr955 [A 9]	OG1	Chl	O	Trp924 [A 8]	Leu951 [A 9]	Thr955 [A 9]	
-7.4	Chl	OH	Gly848 [A 7]	O	Tyr847 [A 7	Gly848 [A 7]	Tyr43 [B]	
	Chl	OH	Tyr847 [A 7]	O				
	Tyr43 [B]	OH	Chl	O				
Pig kidney phosphorylated form with ouabain, 4hyt								
-6.6	Ala925 [A 8]	N	Chl	O	Val921 [A 8]	Trp924 [A 8]	Ala925 [A 8]	
-6.5	Chl	OH	Gly848 [A 7]	O	Tyr847 [A 7]	Gly848 [A 7]	Tyr43 [B]	
	Chl	OH	Tyr43 [B]	OH				
	Chl	OH	Tyr847 [A 7]	O				
	Tyr43 [B]	OH	Chl	O				

E[1]	Donor		Acceptor		Local Residues (within 3 Å of a cholesterol –OH group)			
Shark, 2zxe								
-8.1	Chl	OH	Thr814 [A 6]	O	Gly813 [A 6]	Thr814 [A 6]	Met816 [A 6]	Val817 [A 6] Pro818 [A6]
-6.9	Chl	OH	Ser995 [A 10]	OG	Ser995 [A 10]	Leu996 [A 10]		
-6.6	Chl	OH	Glu960 [A 9]	OE1	Glu960 [A 9]			
-6.3	Chl	OH	Thr138 [A 2]	OG1	Val134 [A 2]	Ser137 [A 2]	Thr138 [A 2]	
Shark complex with ouabain, 3a3y								
-7.6	Chl	OH	Ser995 [A 10]	OG	Ser995 [A 10]	Leu996 [A 10]		
-7.1	Chl	OH	Leu41 [B]	O	Tyr40 [B]	Leu41 [B]	Gly45 [B]	
-7.1	Chl	OH	Ile327 [A 4]	O	Ala299 [A 3]	Ile327 [A 4]		
-6.9	Ala932 [A 8]	N	Chl	O	Val928 [A 8]	Trp931 [A 8]	Ala932 [A 8]	Ser995 [A 10]
Shark with Tl substitution, 5avr								
-8.1	Chl	OH	Ser995 [A 10]	OG	Ser995 [A 10]	Leu996 [A 10]		
Shark with Rb substitution, 5aw4								
-7.6	Chl	OH	Ser995 [A 10]	OG	Ser995 [A 10]	Leu996 [A 10]		
-6.8	Chl	OH	Ser995 [A 10]	OG	Ala932 [A 8]	Ser995 [A 10]	Leu996 [A 10]	

Solute Carrier (SLC) Transporter Superfamily

EAAT1 excitatory amino acid transporter (SLC1), mutant, bound to L-Asp, human, 5llu								
-5.9	Chl	OH	Trp267 [5]	O	Trp267 [5]	Tyr268 [5]	Pro270 [5]	Leu271 [5]
GLUT1 glucose transporter (SLC2), mutant, human, 4pyp								
None								
GLUT1 glucose transporter (SLC2), bound to cytocholasin, human, 5eqi								
-7.1	Chl	OH	Ser73 [2]	OG	Ser73 [2]	Trp412 [11]		
GLUT1 glucose transporter (SLC2), bound to GLUT-i1 inhibitor, human, 5eqg								
-6.6	Chl	OH	Ser73 [2]	OG	Ser73 [2]	Trp412 [11]		
GLUT1 glucose transporter (SLC2), bound to GLUT-i2 inhibitor, human, 5eqh								
-6.6	Chl	OH	Ser73 [2]	OG	Ser73 [2]	Trp412 [11]		
GLUT3 glucose transporter (SLC2), mutant, bound to D-glucose, outward facing form, human, 4zw9								
-6.0	Chl	OH	Thr103 [3]	OG1	Leu99 [3]	Val102 [3]	Thr103 [3]	
-5.8	Chl	OH	Thr441 [12]	OG1	Gly437 [12]	Ile440 [12]	Thr441 [12]	
GLUT3 glucose transporter (SLC2), mutant, bound to maltose, outward facing form, human, 4zwb								
-5.9	Chl	OH	Thr103 [3]	OG1	Leu99 [3]	Thr103 [3]		
-5.9	Chl	OH	Thr441 [12]	OG1	Gly437 [12]	Ile440 [12]	Thr441 [12]	
GLUT3 glucose transporter (SLC2), mutant, bound to D-glucose, outward facing form, human, 4zwc								
-5.7	Chl	OH	Thr103 [3]	OG1	Leu99 [3]	Val102 [3]	Thr103 [3]	
-5.5	Chl	OH	Thr441 [12]	OG1	Gly437 [12]	Phe438 [12]	Thr441 [12]	
GLUT5 fructose transporter (SLC2), open-inward facing form, bovine, 4yb9								
-7.2	Chl	OH	Thr452 [12]	OG1	Ile448 [12]	Thr452 [12]		
-7	Chl	OH	Ser422 [11]	OG	Val418 [11]	Ser422 [11]		
-6.4	Chl	OH	Thr354 [9]	OG1	Thr354 [9]	Ala355 [9]		
GLUT5 fructose transporter (SLC2), open-outward facing form [renumbered to matxh 4yb9], rat, 4ybq								
-6.6	Chl	OH	Ser422 [11]	OG	Val418 [11]	Ser422 [11]		

E^1	Donor	Acceptor	Local Residues (within 3 Å of a cholesterol –OH group)
Erythrocyte Band 3 anion exchange (SLC4), human, 4yzf			
None			

DAT Dopamine transporter (SLC6), bound to antidepressant, Drosophila, 4m48								
None								
DAT Dopamine transporter (SLC6),bound to dopamine, Drosophila, 4xp1								
-7.8	Chl	OH	Ser453 [9]	OG	Ala449 [9]	Phe452 [9]	Ser453 [9]	
-6.7	Chl	OH	Thr535 [11]	OG1	Thr535 [11]			
DAT Dopamine transporter (SLC6),bound to D-amphetamine, Drosophila, 4xp9								
-8.1	Chl	OH	Ser412 [8]	OG	Ala408 [8]	Ser412 [8]		
DAT Dopamine transporter (SLC6),bound to methamphetamine, Drosophila, 4xp6								
-7.6	Chl	OH	Ser453 [9]	OG	Ala449 [9]	Phe452 [9]	Ser453 [9]	
-6.9	Chl	OH	Thr535 [11]	OG1	Leu484 [10]	Thr535 [11]		
DAT Dopamine transporter (SLC6),bound to 3,4-dichlorophenethylamine, Drosophila, 4xpa								
-8	Chl	OH	Ser453 [9]	OG	Ala449 [9]	Phe452 [9]	Ser453 [9]	
DAT Dopamine transporter (SLC6),bound to cocaine, Drosophila, 4xp4								
-7.4	Chl	OH	Ser453 [9]	OG	Ala449 [9]	Ser453 [9]		
DAT Dopamine transporter (SLC6),bound to cocaine analogue, Drosophila, 4xp5								
-6.9	Chl	OH	Ser453 [9]	OG	Ala449 [9]	Phe452 [9]	Ser453 [9]	
DAT Dopamine transporter (SLC6),mutant, bound to cocaine, Drosophila, 4xpb								
-6.5	Chl	OH	Ser566 [12]	OG	Cys562 [12]	Ile563 [12]	Ser566 [12]	
-6.4	Chl	OH	Ser453 [9]	OG	Ala449 [9]	Phe452 [9]	Ser453 [9]	
DAT Dopamine transporter (SLC6),mutant, bound to RTI55, Drosophila, 4xpf								
-7.4	Chl	OH	Thr355 [7]	OG1	Ile351 [7]	Ala354 [7]	Thr355 [7]	
DAT Dopamine transporter (SLC6),mutant, bound to beta-CFT, Drosophila, 4xpg								
-7.8	Chl	OH	Ser453 [9]	OG	Ala449 [9]	Ser453 [9]		
DAT Dopamine transporter (SLC6),mutant, bound to 3,4-dichlorophenethylamine, Drosophila, 4xph								
-7.7	Chl	OH	Ser453 [9]	OG	Ala449 [9]	Ser453 [9]		
-6.9	Chl	OH	Ser482 [10]	PG	Ser482 [10]	Ala564 [12]	Val568 [12]	
DAT Dopamine transporter (SLC6),mutant with 3,4-dichlorophenethylamine, Drosophila, 4xpt								
-7.5	Chl	OH	Ser453 [9]	OG	Ala449 [9]	Phe452 [9]	Ser453 [9]	
DAT Dopamine transporter (SLC6),bound to nisoxetine, Drosophila, 4xnu								
-6.9	Chl	OH	Ser453 [9]	OG	Ala449 [9]	Ser453 [9]		
DAT Dopamine transporter (SLC6),bound to reboxetine, Drosophila, 4xnx								
-7.5	Chl	OH	Ser453 [9]	OG	Ala449 [9]	Ser453 [9]		

Serotonin transporter (SLC6), bound to paroxetine, human, 5i6x								
-8.5	Chl	OH	Thr264 [4]	OG1	Met260 [4]	Thr264 [4]		
-7.7	Chl	OH	Thr503 [10]	OG1	Pro499 [10]	Ala500 [10]	Thr503 [10]	
-7.1	Chl	OH	Thr433 [8]	OG1	Leu429 [8]	Thr433 [8]		
-6.9	Chl	OH	Ser584 [12]	O	Ile167 [3]	Tyr171 [3]	Ser584 [12]	
	Chl	OH	Tyr171 [3]	OH				
Serotonin transporter (SLC6), mutant, bound to s-citalopram, human, 5i71								
-9.1	Chl	OH	Phe263 [4]	O	Met260 [4]	Phe263 [4]	Thr264 [4]	
	Chl	OH	Thr264 [4]	OG1				

E^1	Donor		Acceptor		Local Residues (within 3 Å of a cholesterol –OH group)			
-7.5	Chl	OH	Thr371 [7]	OG1	Val367 [7]	Met370 [7]	Thr371 [7]	
Serotonin transporter (SLC6), mutant, bound to s-citalopram at more sites, human, 5i73								
-9.2	Chl	OH	Phe263 [4]	O	Met260 [4]	Phe263 [4]	Thr264 [4]	
-8.0	Chl	OH	Phe263 [4]	O	Met260 [4]	Phe263 [4]	Thr264 [4]	
	Chl	OH	Thr264 [4]	OG1				
-6.3	Chl	OH	Phe548 [12]	O	Leu547 [12]	Phe548 [12]		
-6.2	Chl	OH	Thr286 [5]	OG1	Val283 [5]	Thr286 [5]	Phe287 [5]	
Serotonin transporter (SLC6), mutant, bound to Br-citalopram, human, 5i74								
-8.5	Chl	OH	Thr264 [4]	OG1	Met260 [4]	Phe263 [4]	Thr264 [4]	
-6.2	Chl	OH	Phe548 [12]	O	Leu547 [12]	Phe548 [12]	Phe551 [12]	
Serotonin transporter (SLC6), mutant, bound to citalopram and Br-citalopram, human, 5i75								
-9.1	Chl	OH	Phe263 [4]	O	Met260 [4]	Phe263 [4]	Thr264 [4]	
	Chl	OH	Thr264 [4]	OG1				
-6.5	Chl	OH	Thr286 [5]	OG1	Val283 [5]	Thr286 [5]	Phe287 [5]	
-6.3	Chl	OH	Phe548 [12]	O	Leu547 [12]	Phe548 [12]		

Antiporters

Mitochondrial ADP/ATP Carrier with carboxyatractyloside, heart, bovine, 1okc								
-6.7	Chl	OH	Ala24 [1]	O	Ala24 [1]			
Mitochondrial ADP/ATP Carrier, with bound cardiolipins, heart, bovine, 2c3e								
-7.3	Chl	OH	Gly224 [5]	O	Gly224 [5]	Ser227 [5]	Tyr228 [5]	
-6.5	Arg234 [5]	NH2	Chl	OH	Leu127 [3]	Ser179 [4]	Arg234 [5]	
	Chl	OH	Ser179 [4]	OG				
-6.3	Chl	OH	Ala24 [1]	O	Ala24 [1]			

ATP Binding Cassette (ABC) Transporters

P-Glycoprotein, nucleotide-free, inward-facing, mouse, 4q9h								
-8.7	His60 [1]	NE2	Chl	OH	His60 [1]	Gln191 [3]	Gln942 [11]	
-8.4	Chl	OH	Tyr303 [5]	OH	Tyr303 [5]	Gln721 [7]		
-6.2	Chl	OH	Thr765 [8]	OG1	Cys713 [7]	Thr765 [8]		
P-Glycoprotein, ATP-bound, outward-facing, human, 6cOv								
-7.4	Chl	OH	Ser222 [4]	OG	Ser222 [4]	Gly226 [4]		
	Ser222 [4]	OG	Chl	OH				
-7.0	Chl	OH	Thr845 [9]	OG1	Ala841 [9]	Thr845 [9]		
-6.5	Chl	OH	Ala987 [9]	O	Asn839 [9]	Ala987 [9]		
MRP-1 drug resistance protein, ATP-bound, outward facing, bovine, 6bhu								
-9.6	Chl	OH	Ser446 [3]	OG	Asp336 [1]	Ser446 [3]	Gln450 [3]	
-7.6	Chl	OH	Thr378 [2]	OG1	Ala374 [2]	Thr378 [2]	Asn1207 [11]	
ABCB10 mitochondrial ABC transporter with bound AMPPC, human, 4ayt								
-8.7	Chl	OH	Ser182 [1]	OG	Leu178 [1]	Ser182 [1]	Arg295 [3]	
-8.7	Chl	OH	Ser326 [4]	OG	Val322 [4]	Val325 [4]	Ser326 [4]	
-8.0	Chl	OH	Ser181 [1]	OG				
	Ser181 [1]	OG	Chl	OH	Ser181 [1]	Ser182 [1]		
-7.9	Chl	OH	Ser301 [3]	OG	Gly297 [3]	Ser301 [3]		

E[1]	Donor		Acceptor		Local Residues (within 3 Å of a cholesterol –OH group)			
ABCB10 mitochondrial ABC transporter with bound AMPPC, rod form, human, 4ayx								
-8.6	Trp440 [6]	NE1	Chl	OH	Gln299 [3]	Trp440 [6]		
-8.6	Chl	OH	Ser182 [1]	OG	Leu178 [1]	Ser181 [1]	Ser182 [1]	
-8.6	Chl	OH	Ser182 [1]	OG	Ser182 [1]	Gln299 [3]		
-8	Chl	OH	Ser181 [1]	OG	Ser181 [1]	Gly225 [2]		
-7.7	Chl	OH	Ser326 [4]	OG	Val322 [4]	Val325 [4]	Ser326 [4]	
ABCB10 mitochondrial ABC transporter with bound AMPPC, plate form, human, 4ayw								
-9.5	Chl	OH	Ser181 [1]	OG	Ser181 [1]	Gly225 [2]		
-9.5	Chl	OH	Ser326 [4]	OG	Val322 [4]	Val325 [4]	Ser326 [4]	
-8.5	Trp440 [6]	NE1	Chl	OH	Ser185 [1]	Gln299 [3]	Trp440 [6]	
ABCB10 mitochondrial ABC transporter, nucleotide-free rod form, human, 3zdq								
-8.4	Chl	OH	Ser181 [1]	OG	Ser181 [1]	Asn229 [2]		
	Ser181 [1]	OG	Chl	OH				
-8.3	Chl	OH	Ser182 [1]	OG	Ser182 [1]	Gln299 [3]		
-8.3	Trp440 [6]	NE1	Chl	OH	Gln299 [3]	Trp440 [6]		

Cystic Fibrosis Transmembrane conductance regulator (CFTR), Zebra fish, 5tsi								
-9.2	Chl	OH	Leu1114 [11]	O	Leu1114 [11]	Phe1115 [11]		
-8.1	Chl	OH	Ser232 [4]	OG	Leu228 [4]	Ser232 [4]		
-7.7	Chl	OH	Glu871 [7]	OE1	Glu871 [7]	Tyr927 [8]	Leu934 [8]	
	Chl	OH	Tyr927 [8]	OH				
-7.5	Chl	OH	Phe313 [5]	O	Ala310 [5]	Phe313 [5]	Ser314 [5]	
-6.9	Arg941 [8]	NH1	Chl	OH	Arg941 [8]			
-6.9	Chl	OH	Thr133 [2]	OG1	Gly129 [2]	Leu130 [2]	Thr133 [2]	
-6.5	Chl	OH	Thr1120 [11]	OG1	Val1116 [11]	Phe1117 [11]	Thr1120 [11]	

1. kcals mol^{-1}, with molar concentration units.

TABLE S4 Other Membrane Proteins

E[1]	Donor		Acceptor		Local Residues (within 3 Å of a cholesterol –OH group)			
Novel Receptors								
STRA6 retinol uptake receptor, zebra fish, 5sy1								
-7.3	Chl	OH	Ser48 [A1]	OG	Ala45 [A1]	Ser48 [A1]	Leu49 [A1]	
-6.4	Chl	OH	Thr133 [A3]	OG1	Leu129 [A3]	Thr133 [A3]		
-6.0	Chl	OH	Ala191 [A5]	O	Ala191 [A5]	Cys192 [A5]		
Tetraspanins								
CD81 tetraspanin, human, 5tcx								
None								
Intramembrane Proteases								
CAAX protease ZMPSTE24, human, 4aw6								
-11.5	Chl	OH	Ser208 [5]	OG	Thr204 [5]	Ser208 [5]	Gln353 [6]	
-11.5	Chl	OH	Thr204 [5]	OG1	Thr204 [5]	Leu205 [5]	Ser208 [5]	Gln353 [6]
-10.6	Chl	OH	Glu86. [2]	OE2	Glu86 [2]	Thr90 [2]		
CAAX protease ZMPSTE24, mutant, complex with tetrapeptide, human, 2ypt								
-11.2	Chl	OH	Ser208 [5]	OG	Thr204 [5]	Ser208 [5]	Gln353 [6]	
-10.1	Chl	OH	Glu86 [2]	OE2	Glu86 [2]	Thr90 [2]		
-8.8	Chl	OH	Ser134 [3]	OG	Ala130 [3]	Thr131 [3]	Ser134 [3]	
-8.4	Chl	OH	Ser208 [5]	OG	Thr204 [5]	Leu205 [5]	Ser208 [5]	Gln353 [6]
	Chl	OH	Thr204 [5]	OG1				
γ-secretase, human, 5a63								
-7.3	Chl	OH	Thr99 [B1]	OG1	Val95 [B1]	Ala98 [B1]	Thr99 [B1]	
-6.4	Chl	OH	Tyr181 [B2]	OH	Thr99 [B1]	Tyr181 [B2]		
	Tyr181 [B2]	OH	Chl	OH				
Membrane-associated proteins in Eicosanoid and Glutathione metabolism proteins (MAPEG)								
Microsomal Glutathione transferase I, rat, 2h8a								
-6.3	Chl	OH	Phe134 [B4]	O	Phe133 [B4]	Phe134 [B4]	Tyr137 [B4]	Gly138 [B4]
-6.2	Chl	OH	Tyr115 [C3]	OH	Tyr115 [C3]			
	Tyr115 [C3]	OH	Chl	OH				
Microsomal prostaglandin E synthase, human, 3dww								
-6.7	His102 [A3]	ND1	Chl	OH	Met101 [A3]	His102 [A3]		
-6.7	Chl	OH	Gln134 [A4]	O	Gln134 [A4]	Cys137 [A4]	Ala138 [A4]	
-6.4	Chl	OH	Leu132 [A4]	O	Val105 [A3]	Gly109 [A3]	Leu132 [A4]	
-6.2	Chl	OH	Ser139 [A4]	OG	Leu135 [A4	Pro136 [A4	Ser139 [A4	
Microsomal prostaglandin E synthase, human, 4al0								
None								
5-lipoxygenase-activating protein, human, 2q7m								
None								
Leukotriene LTC-4 synthase, human, 2pno								
None								
Leukotriene LTC-4 synthase, human, 2uuh								
None								

E^1	Donor	Acceptor	Local Residues (within 3 Å of a cholesterol –OH group)
LeukotrieneLTC-4 synthase with bound leukotriene analog I, human, 4jcz			
None			
LeukotrieneLTC-4 synthase mutant with bound leukotriene analog I, human, 4jrz			
None			
LeukotrieneLTC-4 synthase with bound leukotriene analog II, human, 4j7t			
None			
LeukotrieneLTC-4 synthase with bound leukotriene analog III, human, 4j7y			
None			

Sterol-Sensing Domain (SSD) Proteins

Niemann-Pick C1 protein, human, 5u73								
-6.5	Chl	OH	Thr743 [6]	OG1	Thr743 [6]	Val744 [6]		
-6.0	Ser666 [4]	OG	Chl	OH	Leu662 [4]	Ile663 [4]	Ser666 [4]	
Niemann-Pick C1 protein, human, 5u74								
-6.6	Chl	OH	His1239 [13]	ND1	Thr1238 [13]	His1239 [13]		
-6.4	Ser666 [4]	OG	Chl	OH	Leu662 [4]	Ser666 [4]		
-6.2	Chl	OH	Thr743 [6]	OG1	Phe740 [6]	Thr743 [6]	Val744 [6]	

Palmitoyl Transferase

Palmitoyl transferase, human, 6bml								
None								
Palmitoyl transferase, human, 6bmm								
-5.9	Chl	OH	Thr23 [1]	OG1	Thr23 [1]			
Palmitoyl transferase, human, 6bmn								
-5.5	Chl	OH	Thr23 [1]	OG1	Val19 [1]	Leu20 [1]	Thr23 [1]	

Fatty Acid Desaturase

Stearoyl-coenzyme A desaturase (SCD1), with substrate, human, 4zyo: ih, inner helix								
-7.7	Chl	OH	Tyr108 [2]	OH	Tyr108 [2]	Leu290 [ih]	Gly291 [ih]	
-7.2	Chl	OH	Thr231 [3]	OG1	Phe227 [3]	Thr231 [3]	Thr250 [4]	
Stearoyl-coenzyme A desaturase (SCD1), with substrate, mouse, 4ymk								
-7.2	Chl	OH	Thr106 [2]	OG1	Phe102 [2]	Met105 [2]	Thr106 [2]	

Hydrolases

Estrone sulphatase, placenta, human, 1p49								
-5.9	Chl	OH	Thr196 [1]	OG1	Ile192 [1]	Thr196 [1]		

Electron Transport Chain Complex II

Succinate:ubiquinone oxidoreductase (SQR, Complex II), heart, chicken, 2fbw								
-5.7	Chl	OH	Ala90 [C2]	O	Ala90 [C2]	Leu91 [C2]	Pro94 [C2]	
	Chl	OH	Leu91 [C2]	O				
Succinate:ubiquinone oxidoreductase (SQR, Complex II) with TEO, heart, chicken, 2h88								
None								
Succinate:ubiquinone oxidoreductase (SQR, Complex II), heart, pig, 1zoy								
-8.6	Chl	OH	Thr77 D2]	OG1	Ala74 [D2]	Thr77 [D2]	Leu78 [D2]	

E^1	Donor		Acceptor		Local Residues (within 3 Å of a cholesterol –OH group)			
Succinate:ubiquinone oxidoreductase (SQR, Complex II), chicken, 1yq3								
-5.7	Chl	OH	Tyr73 D3]	OH	Tyr73 [D3]			
	Tyr73 [D3]	OH	Chl	OH				
Succinate:ubiquinone oxidoreductase (SQR, Complex II), worm, 3vr8								
-7.2	Chl	OH	Thr132 [C2]	OG1	Ile128 [C2]	Ala129 [C2]	Thr132 [C2]	
-6.4	Chl	OH	Thr85 [C1]	OG1	Ala81 [C1]	Thr85 [C1]		
	Thr85 [C1]	OG1	Chl	OH				
-6.0	Chl	OH	Ile123 [C2]	O	Ile123 [C2]	Ile124 [C2]		
	Chl	OH	Ile124 [C2]	O				

Electron Transport Chain Complex III (Cytochrome bc1)

Cytochrome bc1, bovine heart,1bgy								
-9.6	Chl	OH	Tyr358 [C8]	OH	Ser297 [C6]	Tyr358 [C8]		
-8.1	Ser34 [K1]	OG	Chl	OH	Val25 [J1]	Ala28 [J1]	Leu29 [J1]	Ser34 [K1]
-7.8	Chl	OH	Thr334 [C7]	OG1	Ala330 [C7]	Asp331 [C7]	Thr334 [C7]	
Cytochrome bc1, bovine heart,[subunits renamed to match 1bgy],1pp9								
-7.5	Chl	OH	Asp331 [C7]	OD1	Ala330 [C7]	Asp331 [C7]	Thr334 [C7]	
-7.2	Chl	OH	Tyr358 [C8]	OH	Ser297 [C6]	Tyr358 [C8]		
-7.1	Chl	OH	Thr42 [E1]	OG1	Thr42 [E1]			
Cytochrome bc1, bovine heart,[subunits renamed to match 1bgy],5nmi								
-8.0	Chl	OH	Ser34 [K1]	OG	Gly31 [K1]	Ser34 [K1]	Ala35 [K1]	
	Ser34 [K1]	OG	Chl	OH				
Cytochrome bc1, with inhibitor, bovine heart,2fyu								
-8.8	Chl	OH	Tyr358 [C8]	OH	Ser297 [C6]	Tyr358 [C8]		
-7.9	Chl	OH	Asp331 [C7]	OD2	Ala330 [C7]	Asp331 [C7]	Thr334 [C7]	
Cytochrome bc1, bovine heart,[subunits renamed to match 1bgy], 1ntm								
-8.6	Chl	OH	Tyr358 [C8]	OH	Ser297 [C6]	Ile298 [C6]	Tyr358 [C8]	
Cytochrome bc1, bovine heart,[subunits renamed to match 1bgy], 1l0l								
-9.0	Chl	OH	Tyr358 [C8]	OH	Ser297 [C6]	Leu301 [C6]	Tyr358 [C8]	
-8.0	Chl	OH	Asp331 [C7]	OD1	Ala330 [C7]	Asp331 [C7]	Thr334 [C7]	
-8.0	Chl	OH	Thr44 [E1]	OG1	Thr44 [E1]	Ala48 [E1]		
Cytochrome bc1, human, [subunits renamed to match 1bgy],5xte								
-8.1	Chl	OH	Ala126 [E1]	O	Ala126 [E1]	Lys130 [E1]		
-6.9	Chl	OH	Ser238 [C5]	OG	Leu234 [C5]	Phe235 [C5]	Ser238 [C5]	

Electron Transport Chain Complex IV (Cytochrome c Oxidase)

Cytochrome c oxidase, fully oxidised, [early structure], bovine heart, 1occ								
-7.2	Chl	OH	Ser27 [G1]	OG	Leu23 [G1]	Ala24 [G1]	Ser27 [G1]	
-7.1	Chl	OH	His151 [A4]	ND1	His151 [A4]	Thr207 [A5]		
-7.0	Chl	OH	Thr48 [C2]	OG1	Met44 [C2]	Thr48 [C2]		
-6.9	Chl	OH	Thr95 [C3]	OG1	Val91 [C3]	Thr95 [C3]		

E[1]	Donor		Acceptor		Local Residues (within 3 Å of a cholesterol –OH group)			
Cytochrome c oxidase, fully oxidised, bovine heart, 1v54								
-8.5	Chl	OH	Ser89 [C3]	OG	Ser89 [C3]	Glu90 [C3]		
-7.6	Chl	OH	Thr174 [C5]	OG1	Gly170 [C5]	Val171 [C5]	Thr174 [C5]	Ser212 [C6]
-7.3	Chl	OH	Thr48 [C2]	OG1	Met44 [C2]	Thr48 [C2]		
-7.2	Chl	OH	Ser28 [I1]	OG	Ala24 [I1]	Ser28 [I1]		
Cytochrome c oxidase, fully reduced, bovine heart, 1v55								
-8.4	Chl	OH	Ser89 [C3]	OG	Ser89 [C3]			
-7.8	Chl	OH	Ser212 [C6]	OG	Gly170 [C5]	Thr174 [C5]	Ser212 [C6]	
	Chl	OH	Thr174 [C5]	OG1				
-7.4	Chl	OH	Thr48 [C2]	OG1	Met44 [C2]	Leu47 [C2]	Thr48 [C2]	
-7.2	Chl	OH	Ser27 [G1]	OG	Leu23 [G1]	Ala24 [G1]	Ser27 [G1]	
Cytochrome c oxidase, with bound cyanide, bovine heart, 3x2q								
-8.3	Chl	OH	Ser89 [C3]	OG	Ser89 [C3]	Glu90 [C3]		
-7.2	Chl	OH	Thr48 [C2]	OG1	Met44 [C2]	Thr48 [C2]		
-7.2	Chl	OH	Ser212 [C6]	OG	Gly170 [C5]	Thr174 [C5]	Ser212 [C6]	
	Chl	OH	Thr174 [C5]	OG1				
-7.0	Chl	OH	Ser28 [I1]	OG	Ala24 [I1]	Ser28 [I1]		
-7.0	Chl	OH	Ser27 [G1]	OG	Leu23 [G1]	Ala24 [G1]	Ser27 [G1]	
Cytochrome c oxidase, with bound cytochrome c, bovine heart, 5iy5								
-8.8	Chl	OH	Ser89 [C3]	OG	Ser89 [C3]			
-7.8	Chl	OH	Ser212 [C6]	OG	Gly170 [C5]	Thr174 [C5]	Ser212 [C6]	
	Chl	OH	Thr174 [C5]	OG1				
-7.2	Chl	OH	Thr48 [C2]	OG1	Met44 [C2]	Leu47 [C2]	Thr48 [C2]	
Cytochrome c oxidase, at neutral pH, bovine heart, 5xdq								
-8.6	Chl	OH	Ser89 [C3]	OG	Ser89 [C3]			
-8.2	Chl	OH	Ser212 [C6]	OG	Gly170 [C5]	Thr174 [C5]	Ser212 [C6]	
	Chl	OH	Thr174 [C5]	OG1				
-7.6	Chl	OH	Thr48 [C2]	OG1	Met44 [C2]	Thr48 [C2]		

1. kcals mol^{-1}, with molar concentration units.

TABLE S5 Residues interacting with cholesterol in more than two members of the Class A GPCRs

No.[1]	Residue	GPCR
1.43	Ser	mAChR M1, M2, M4
2.54	Ser, Gly	$5HT_{1B}$, $A2_a$, mAChR M3
2.55	Val, Ser, Leu	$A2_a$, Opioid μ, $P2Y_{12}$
3.34	Tyr	NOP, Opioid δ, κ, μ
5.46 + 5.461	Ala, Cys,Val	$5HT_{1B}$, $A2_a$, β_2AR, mAChR M1, M3, M4
6.46 + 6.461	Ala, Leu, Phe	CXC4, FFAR1, AT1
6.47	Cys, Ser	CXC4, $P2Y_1$, AT1
7.47	Gly, Thr, Ser	β_2AR, CB_1, Opioid δ, κ

1. Residue number in the Ballesteros-Weinstein numbering system (1).

SUPPORTING REFERENCES

1. Ballesteros, J. A., and H. Weinstein. 1995. Integrated methods for the construction of three-dimensional models and computational probing of structre-fiunction relations in G protein-coupled receptors. In Methods in Neurosciences Vol. 25. C. S. Stuart, editor. Academic Press, San Diego. 366-428.
2. Wootten, D., J. Simms, L. J. Miller, A. Christopoulos, and P. M. Sexton. 2013. Polar transmembrane interactions drive formation of ligand-specific and signal pathway-biased family B G protein-coupled receptor conformations. Proc. Natl. Acad. Sci. USA 110:5211-5216.
3. Pin, J.-P., T. Galvez, and L. Prézeau. 2003. Evolution, structure, and activation mechanism of family 3/C G-protein-coupled receptors. Pharmacology & Therapeutics 98:325-354.
4. Wang, C., H. Wu, T. Evron, E. Vardy, G. W. Han, X.-P. Huang, S. J. Hufeisen, T. J. Mangano, D. J. Urban, V. Katritch, V. Cherezov, M. G. Caron, B. L. Roth, and R. C. Stevens. 2014. Structural basis for Smoothened receptor modulation and chemoresistance to anticancer drugs. Nature Comm. 5:4355.